

Changes in blast zone albedo patterns around new martian impact craters



I.J. Daubar^{a,b,*}, C.M. Dundas^c, S. Byrne^b, P. Geissler^c, G.D. Bart^d, A.S. McEwen^b, P.S. Russell^e, M. Chojnacki^b, M.P. Golombek^a

^aJet Propulsion Laboratory, California Institute of Technology, Pasadena, CA 91109, USA

^bLunar and Planetary Laboratory, University of Arizona, Tucson, AZ 85721, USA

^cU.S. Geological Survey, Astrogeology Science Center, 2255 N. Gemini Dr., Flagstaff, AZ 86001, USA

^dUniversity of Idaho, Department of Physics, 875 Perimeter Dr., MS 0903, Moscow, ID 83843, USA

^eNational Air & Space Museum, Smithsonian Institution, MRC 315, P.O. Box 37012, Washington, DC 20013-7012, USA

ARTICLE INFO

Article history:

Received 10 July 2015

Revised 4 November 2015

Accepted 21 November 2015

Available online 15 December 2015

Keywords:

Impact processes

Aeolian processes

Cratering

Mars

Mars, surface

ABSTRACT

“Blast zones” (BZs) around new martian craters comprise various albedo features caused by the initial impact, including diffuse halos, extended linear and arcuate rays, secondary craters, ejecta patterns, and dust avalanches. We examined these features for changes in repeat images separated by up to four Mars years. Here we present the first comprehensive survey of the qualitative and quantitative changes observed in impact blast zones over time. Such changes are most likely due to airfall of high-albedo dust restoring darkened areas to their original albedo, the albedo of adjacent non-impacted surfaces. Although some sites show drastic changes over short timescales, nearly half of the sites show no obvious changes over several Mars years. Albedo changes are more likely to occur at higher-latitude sites, lower-elevation sites, and at sites with smaller central craters. No correlation was seen between amount of change and Dust Cover Index, relative halo size, or historical regional albedo changes. Quantitative albedo measurements of the diffuse dark halos relative to their surroundings yielded estimates of fading lifetimes for these features. The average lifetime among sites with measurable fading is ~ 15 Mars years; the median is ~ 8 Mars years for a linear brightening. However, at approximately half of sites with three or more repeat images, a nonlinear function with rapid initial fading followed by a slow increase in albedo provides a better fit to the fading behavior; this would predict even longer lifetimes. The predicted lifetimes of BZs are comparable to those of slope streaks, and considered representative of fading by global atmospheric dust deposition; they last significantly longer than dust devil or rover tracks, albedo features that are erased by different processes. These relatively long lifetimes indicate that the measurement of the current impact rate by Daubar et al. (Daubar, I.J. et al. [2013]. *Icarus* 225, 506–516. <http://dx.doi.org/10.1016/j.icarus.2013.04.009>) does not suffer significantly from overall under-sampling due to blast zones fading before new impact sites can be initially discovered. However, the prevalence of changes seen around smaller craters may explain in part their shallower size frequency distribution.

© 2015 Elsevier Inc. All rights reserved.

1. Introduction

Signs of past aeolian modification are ubiquitous on Mars: vast sand sheets, wind-scoured plains, and huge deposits of dust. Current aeolian processes are now being observed at the orbital (km) as well as the lander (m) scale (e.g., Bridges et al., 2013; Geissler et al., 2010; Silvestro et al., 2010). These processes are potentially a significant part of the martian dust cycle, with

implications for the generation and recurrence of regional and global dust storms (e.g., Cantor, 2007). Here we investigate these processes by looking at the changes over time of blast zones (BZs), the albedo patterns that surround new impact sites. These BZs are the product of martian impact events detected in the past decade, with formation dates constrained by before-and-after images (Daubar et al., 2013; Malin et al., 2006). They are the freshest available examples of impact processes outside the laboratory, and for the purposes of aeolian studies, they are recently-modified surfaces in dusty areas of Mars with constrained dates for the initial disturbances. Sites where the surface has recently been disturbed are expected to show more physical changes; this has been

* Corresponding author at: Jet Propulsion Laboratory, California Institute of Technology, Pasadena, CA 91109, USA.

E-mail address: ingrid.daubar@jpl.nasa.gov (I.J. Daubar).

demonstrated in areas disturbed by the wheels of the Mars Exploration Rover (MER) Opportunity rover (Chojnacki et al., 2014; Geissler et al., 2010; Johnson et al., 2012). Thus we examine the surroundings of these recently-formed craters for changes over time to improve our understanding of current aeolian processes on dusty surfaces such as the fallout of atmospheric dust, processes which are widespread on Mars.

The High Resolution Imaging Science Experiment (HiRISE) (McEwen et al., 2007) on the Mars Reconnaissance Orbiter (MRO) has now been monitoring many of these impact sites for over 3 Mars years. The rates and characteristics of changes at these locations will help shed light on the effects of the initial impact, the modification processes that have occurred since, and the ultimate fate of these features.

An additional motivation for this study is to determine whether the cratering rate measured by Daubar et al. (2013) might be incorrect because of under-counting new impacts due to fading. Here we examine the possibility that these impact sites are disappearing over short timescales. If the timescales of this process are sufficiently short, the martian cratering rate calculated by Daubar et al. (2013) may be artificially low due to new impacts not being discovered before they fade.

2. Descriptions of impact blast zones

Almost all known new impacts initially have an extended, usually lower, albedo pattern surrounding the craters (Malin et al., 2006; Daubar et al., 2013). Although most features are darker than their surroundings, there are examples of higher-albedo blast zones and sites with both higher- and lower-albedo components relative to pre-existing or adjacent surfaces. The prevalence of lower-albedo features surrounding new impacts is a direct result of the detection technique (Daubar et al., 2013): over bright dusty areas, medium-resolution (6 m/px) repeat imaging by the MRO Context Camera (CTX) (Malin et al., 2007) is able to detect darker spots typical of new impacts. Follow-up imaging by HiRISE confirms an impact occurred and provides details of the new craters and albedo

patterns surrounding them. These darkened areas have been said to be a distinguishing characteristic of primary craters (Calef et al., 2009) in dusty areas, but we observe similar low-albedo patterns around secondaries of these new dated impacts as well.

Markings within the impact area vary widely between sites. One of the most common features is a diffuse, low-albedo “halo” (Fig. 1). Selected halos have been measured to have diameters that range from 7 to 220 times larger than the diameters of the craters themselves (Bart et al., in preparation), and up to 400 times larger at some sites (Ivanov et al., 2010), although the method of defining the gradual halo boundary differs between studies. Other albedo features include arcuate, parabolic, or radial rays (Fig. 2); light and dark-toned ejecta-like patterns (Fig. 3); dust avalanches/slope streaks triggered by the impact (Fig. 4; similar features were also studied by Chuang et al. (2007) and Burleigh et al. (2012)); and complex combinations thereof. We discuss albedo features only, because most of the new impact sites do not have visible ejecta with enough relief to be detectable by HiRISE. Impact-related features outside the central crater are almost exclusively albedo markings, rather than topographic features indicative of significant deposition or erosion. This was also observed by Calef et al. (2009) with a smaller set of new dated impacts. The rare exceptions to this are (1) a few sites where many small slope streaks define the blast zone (Fig. 4)—these remove a thin layer of material, which can be detected when illumination angles are large; (2) several craters (out of almost 500 dated impact sites) with resolvable ejecta blocks near the rim; and (3) a single site with icy blocks observed to sublimate away (Dundas et al., 2014). It is possible that sub-resolution changes in topographic roughness could be producing changes in apparent albedo, and this type of change may be especially slow to disappear. Differing grain sizes or compositional differences could also be playing a part in the observed albedo patterns.

Many formation mechanisms have been hypothesized for the disparate features surrounding the new impacts. The most probable is removal and/or disturbance of high-albedo surface dust by some combination of atmosphere/surface interactions of the shock waves associated with the descent and impact of the bolide and/or

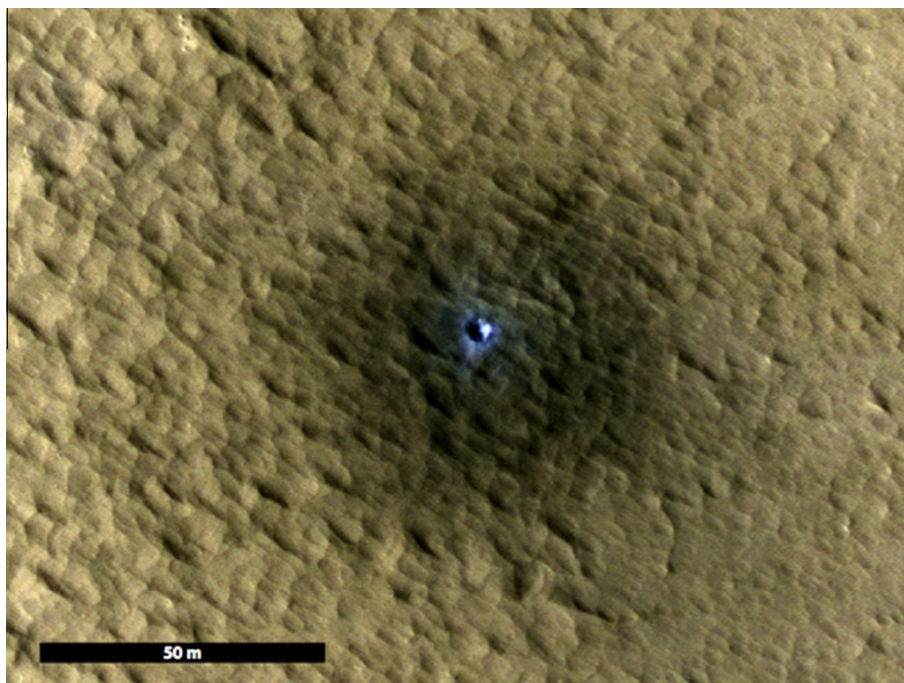


Fig. 1. New dated impact site with diffuse low-albedo “halo” around crater. HiRISE observation ID ESP_020787_1805 at 0.372°N (planetocentric), 284.325°E. In all image figures, HiRISE images are cut out of color (IRB) or red RDRs, reprojected so that north is up, and stretched for contrast; illumination is roughly from the left; scale is 0.25 m/pixel. All HiRISE images credit NASA/JPL/University of Arizona; original data are available via the Planetary Data System.

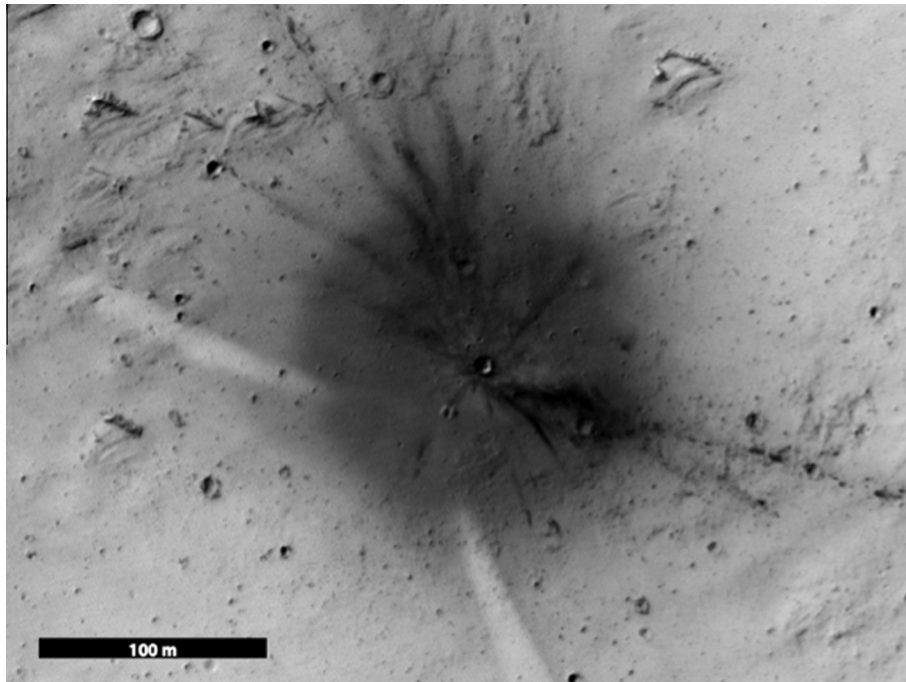


Fig. 2. New dated impact site with complex blast zone including a diffuse low-albedo halo, extended straight low-albedo rays, high-albedo arcuate rays, and outer low-albedo spots and elongate splotches. HiRISE observation ID ESP_034372_1665 at -13.24°N , 200.72°E .

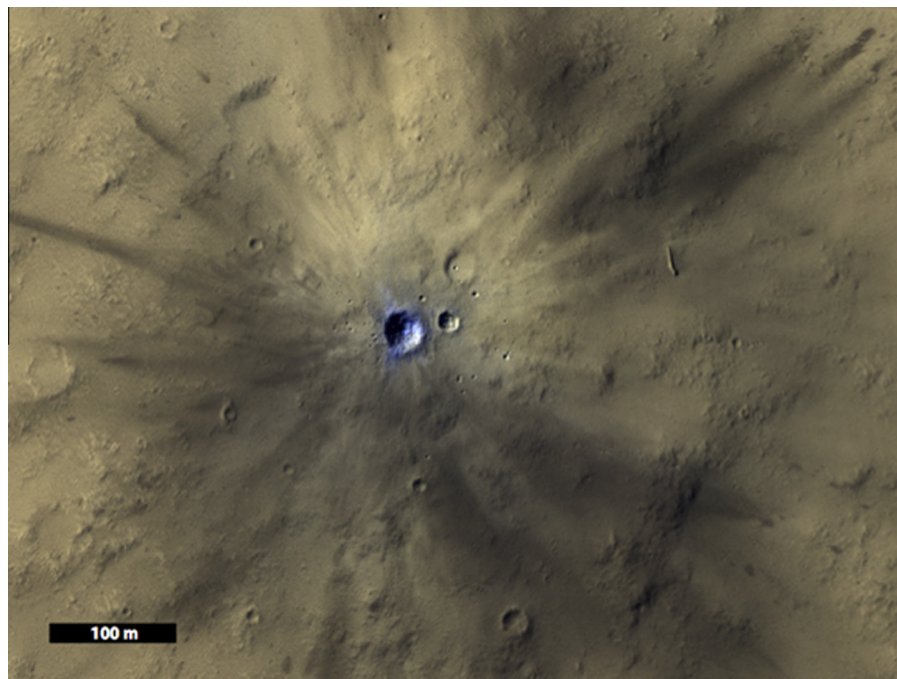


Fig. 3. New dated impact site with dual-toned blast zone including both high-albedo inner rays and low-albedo rays that extend farther from the center. HiRISE observation ID PSP_009265_1730 at -7.05°N , 210.26°E .

ejecta (Malin et al., 2006). Other possibilities include impact ejecta processes (depositional and/or erosional); shock effects on small-scale surface texture that affect roughness; and interactions between shock waves from separated fragments of an impactor (Ivanov et al., 2010). The airblast associated with the impact has also been inferred to cause tens of thousands of small low-albedo dust avalanches at one site in particular, and similar processes have likely contributed to the formation of dark areas at $\sim 8\%$ of new impact sites (Burleigh et al., 2012; Chuang et al., 2007); an example of this can be seen in Fig. 4.

These various types of features may very well have different formation mechanisms, styles and rates of changing albedo over time, and lifetimes before they are no longer visible. We use the general term “blast zone” (BZ) (Malin et al., 2006) to encompass all of these albedo patterns whose formation is associated with the initial impact, without implying a specific formation process, or that they all share a single formation process. This term has also been used to describe areas disturbed by rocket exhaust at lunar and martian landing sites (e.g., Clegg et al., 2014; Johnson et al., 2015), which are also generally low albedo features on Mars

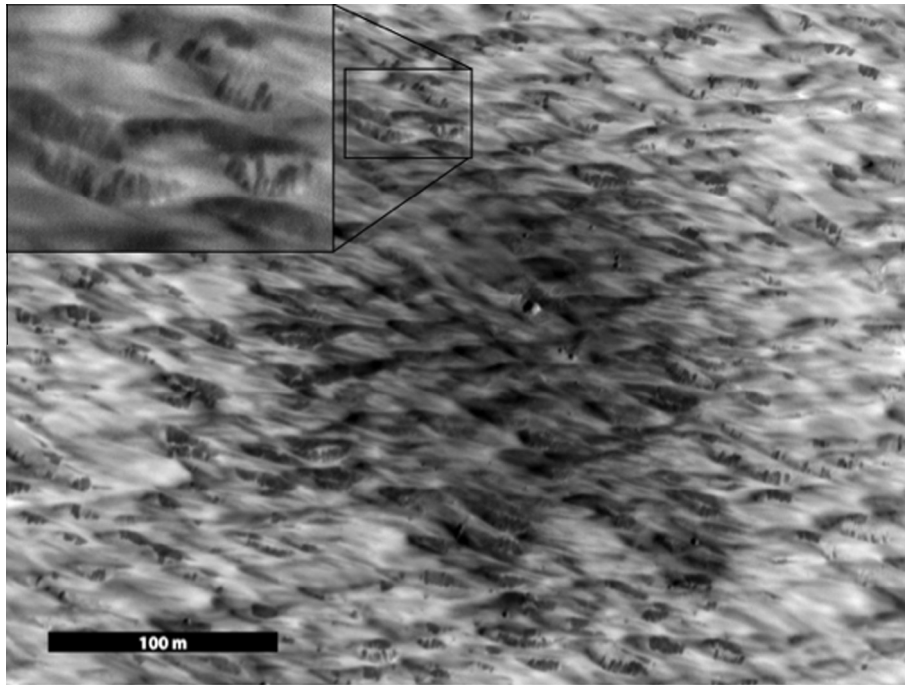


Fig. 4. New dated impact site with small (\sim meter-scale) dust avalanches occurring more densely at closer proximity to the new craters, indicating they were most likely caused by the impact event (Burleigh et al., 2012). HiRISE observation ID ESP_033316_1805 at 0.56°N , 228.31°E . Inset shows dust avalanches in more detail.

(e.g., Daubar et al., 2015; Mehta et al., 2011; Mellon et al., 2009), although they can have both high- and low-albedo zones on the Moon (Clegg et al., 2014). The formation of those lander-generated albedo patterns may or may not involve the same mechanisms as the formation of the impact BZs we describe here.

In continuing HiRISE coverage, we have observed changes in these impact BZ features over time. Byrne et al. (2009) reported some brightening in blast zones, even in closely-spaced repeat images of ice-exposing impacts (Byrne et al., 2009, Supplement). Similar fading of a dark impact BZ was first observed with the Mars Orbital Camera (MOC) in 2005, as discussed in a press release (http://www.msss.com/mars_images/moc/2005/09/20/ulysses_crater/index.html). In that case, the initial BZ albedo was estimated by comparison with other albedo features such as slope streaks and dust devil tracks. However, those features themselves vary widely in their albedos, so we measure the albedo of BZs relative to apparently static surroundings, and the changes in that relative albedo over time, in order to estimate lifetimes for these features.

Previously it was reported that out of 14 sites observed before and after the 2007 global dust storm, surprisingly only one site showed significant BZ changes (Fig. 5 and Geissler and Daubar, 2010). With more than 500 known impacts and many more repeat images, we can now include a significant number of sites with different ages, target materials, and types of blast features. In this paper, we studied 253 images at 106 sites with repeat images ranging up to 4 Mars years apart. To evaluate the changes in BZs over time, we made qualitative assessments of the amount of change at each site, and we measured the albedo relative to the background over time of diffuse halos at selected sites.

3. Methods

3.1. Qualitative assessment of change

We assessed the degree of change at 106 new impact sites with repeat imaging. The entire set of \sim 500 known new dated

craters could not be examined for changes because not all of them have been imaged by HiRISE multiple times under suitable conditions. This subset of known impact sites has the required repeat imaging and meet the following criteria. We limited our study to sites equatorward of 50° north or south latitude and without exposed subsurface ice, because in polar regions different processes are at work erasing BZs on seasonal timescales, e.g., carbon dioxide, dust, and water ice deposition and polar cap sublimation (Dundas et al., 2014). These processes might occur slightly equatorward of 50° , but this cutoff was considered a reasonable limit for the majority of polar processes. Images spaced too closely in time are less likely to show changes, therefore images taken less than 100 days apart were not included in our statistics. Our qualitative assessment from visually examining the few examples of closely spaced images is that any changes they show are non-existent or questionable (change levels 0 or 1 as defined below).

Images were manually coregistered and stretched to match color, brightness, and contrast of background areas, which normalizes some of the effects of images taken at different photometric angles and atmospheric dust opacities. Successive images should appear different if the atmospheric opacity is different at the time of imaging, so it is possible that normalizing to the background masks some real surface changes. Thus changes in opacity between images could result in seeing no changes where subtle changes existed. However, those two classes of change (no changes and subtle changes) were grouped together in our statistical analysis, thus this is not a major concern in the qualitative assessment. Very high opacity images, resulting in very poor surface contrast, were excluded from analysis.

Changes were assessed by blinking between images, and each site was classified into one of these categories: change level 0: no detectable changes; change level 1: subtle changes that may be due to differences in lighting or viewing angles, atmospheric effects, or imperfect image stretching; change level 2: definite changes; change level 3: significant changes (e.g., the BZ has

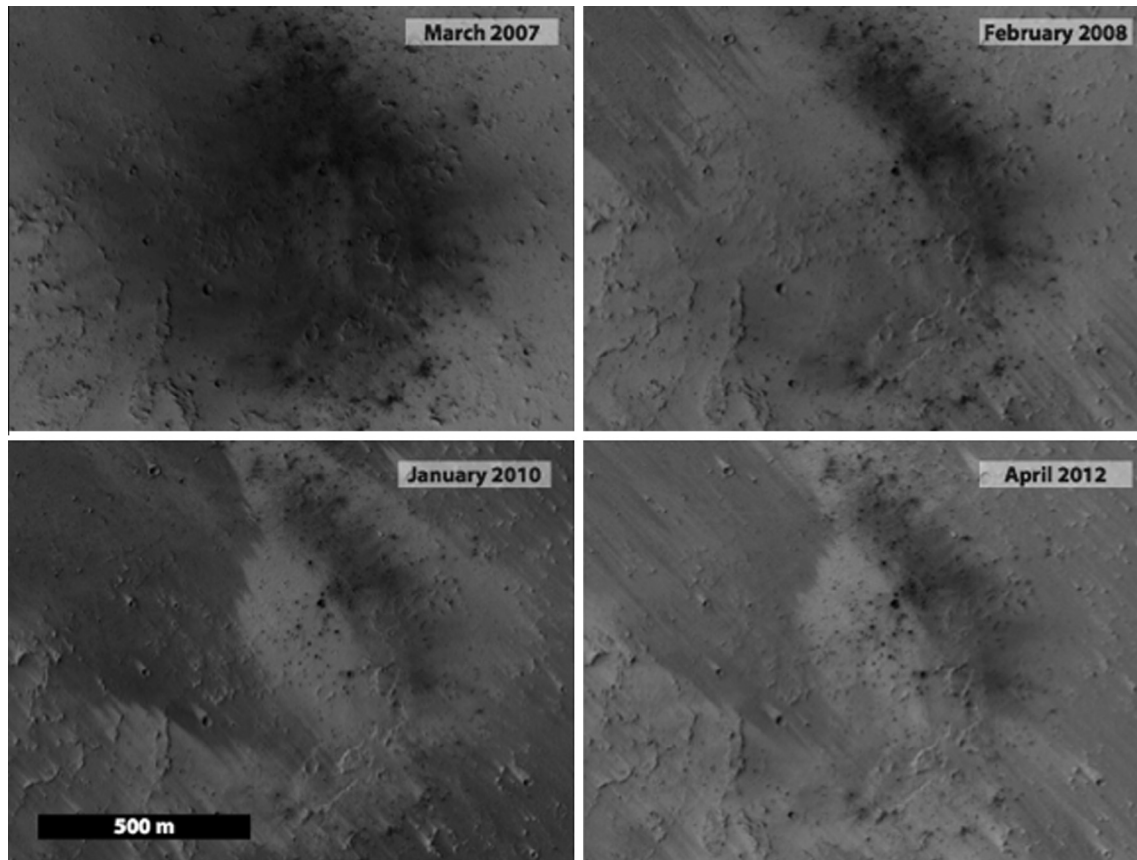


Fig. 5. New impact site showing drastic changes in albedo over 3 Mars years. HiRISE observation IDs (in time order from upper left to lower right) PSP_003172_1870 (3/31/2007), PSP_007431_1870 (2/26/2008), ESP_016160_1870 (1/6/2010), and ESP_026643_1870 (4/2/2012), at 7.00°N, 247.92°E.

disappeared entirely). Examples of these categories are shown in Fig. 6. Qualitative changes were evaluated based on all features within the BZ, not just the diffuse halos on which the quantitative study was focused (Section 3.2).

Correlations between these change rankings and various factors were assessed using the Interactive Data Language (IDL; <http://www.exelisvis.com/IDL>¹) function RS_TEST. This function uses the Mann–Whitney *U* Test to assess whether two sets of sites come from the same population by calculating the probability of them having the same median of distribution. For more details, see the IDL program documentation. A correlation is considered to be found if the test shows that the distribution of sites that displayed change level 0 or 1 is different than the distribution of those with change level 2 or 3 to a confidence level of greater than 95%. The results of this study are reported in Section 4.2.

3.2. Quantitative measurements of change

To measure the fading rates of BZ features, we made quantitative measurements of the relative albedo in repeat images at 70 sites. This data set is smaller than that used for qualitative studies because we focused this study on the dark, diffuse halos around new craters. Those are the most ubiquitous features within BZs, and the most appropriate features for this type of measurement, but are not present at all sites. Sites displaying all qualitative change levels were included to get a wide sampling of fading rates.

To avoid seasonal variations in both real surface albedo and changing viewing conditions, we used HiRISE images of the new

impact sites that were acquired in the same season in successive Mars years. Similar image campaigns have been used successfully for other change detection studies on Mars (e.g., Bridges et al., 2012; Geissler et al., 2013). MRO is in a Sun-synchronous orbit maintaining roughly the same local time of day (~3 p.m.) since the beginning of the Primary Science Phase, but varying with seasons (Zurek and Smrekar, 2007). Thus restricting images to similar seasons also limits them to have similar local times of day and solar azimuth angles. Ideally repeat images would be targeted to be $\pm 10^\circ$ Solar Longitude (L_s) of each other. In practice, not all images could be acquired that close in season, so the difference in L_s between images ranges from 0.1° to 52.0° , averaging 11.8° . Viewing geometries of the repeat images used in this study were as similar as possible; images were all taken on small rolls ($<9^\circ$ off-nadir), and subsequent images' solar incidence angles do not vary widely. The difference between incidence angles at which successive images were taken averaged 2.2° , ranging from 0.05° to 10.8° ; 90% differed by less than 4.7° .

It is a difficult challenge to perform quantitative photometry on HiRISE data (Delamere et al., 2010). We have developed the following technique to measure changing albedos in successive images, which addresses some of these challenges. Images were analyzed using the publicly available HiView software (<http://www.uahirise.org/hiview/>). Two representative regions of interest (ROI) within the low-albedo halo were sampled in HiRISE RED (570–830 nm) Reduced Data Record (RDR) products, and the mean pixel data number (DN) values were obtained for each ROI. ROIs were chosen to include areas uniformly darkened by the impact event, and to exclude significant variations in topography, albedo, or any geographic features that would create shadows or otherwise complicate the albedo measurements. The darkest area of the BZ

¹ The use of brand names is for identification purposes and does not constitute an endorsement.

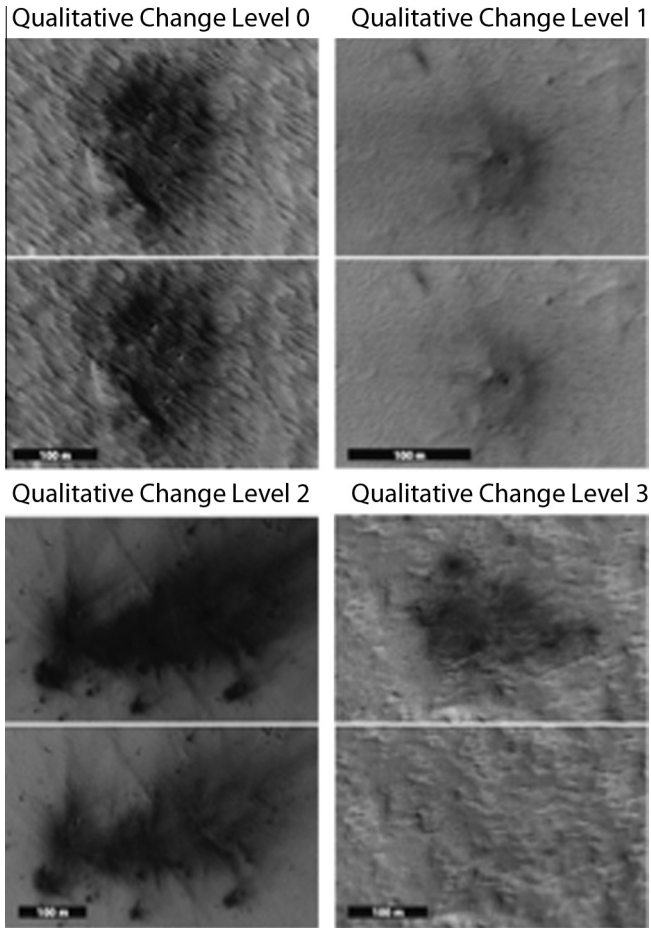


Fig. 6. Examples of qualitative change levels, with earlier (top) and later (bottom) images showing relative levels of change. Change level 0: no discernible changes [HiRISE observation IDs PSP_007378_1860 (2/22/2008) (top) and ESP_034093_1860 (11/4/2013) (bottom) at 6.118°N, 254.341°E]; change level 1: subtle changes [HiRISE observation IDs PSP_008300_1905 (5/4/2008) (top) and ESP_034936_1905 (1/8/2014) (bottom) at 10.420°N, 278.408°E]; change level 2: definite changes [HiRISE observation IDs ESP_014010_1800 (7/23/2009) (top) and ESP_031917_1800 (5/18/2013) (bottom) at 0.160°N, 263.752°E]; change level 3: significant changes [HiRISE observation IDs ESP_013707_1915 (6/29/2009) (top) and ESP_031047_1915 (3/11/2013) (bottom) at 11.476°N, 255.011°E].

meeting those criteria was chosen; where there were two distinct albedo regions, each was sampled. BZ ROI sizes varied widely depending on the size of the blast zone and details of topography, but averaged 4103 pixels (the smallest was 32 pixels). The same areas were sampled in successive overlapping images of the same site. To avoid error due to offsets in geometric projections, the ROI locations were not chosen based on their coordinates, which can result in offsets of tens to hundreds of meters, but instead matched between images by visually georeferencing them to geographic landmarks. The same procedure was performed for another ROI sampling a smooth, flat, featureless surface at sufficient distance from the impact that the surface albedo was not visibly affected by the blast – this is the “background” (BK) sample. Just as with the BZ samples, BK ROIs were chosen where possible to avoid topographic features with shadows that might cause problems with image-to-image comparisons with different lighting conditions or albedo features such as dust devil tracks or wind streaks that may change between images independently of the BZ. See Fig. 7 for an illustration of the sampling locations for an example site.

The total signal incident on the HiRISE focal plane includes contributions from multiple sources:

$$I_r = S_i T_d A T_u + D A T_u + Z \quad (1)$$

where

I_r = flux incident on the detector,

S_i = incident sunlight at the top of the atmosphere at the angle of incidence, i ,

T_d = downward transmission factor (dependent on incidence angle); fraction (<1) of sunlight transmitted through the atmosphere downward to the surface from the top of the atmosphere,

A = albedo of the surface,

T_u = upward transmission factor (dependent on emission angle); fraction (<1) of reflected light transmitted through the atmosphere upward from the surface to the top of the atmosphere,

Z = upward atmospheric scattering into the detector,

D = diffuse illumination of the surface from skylight (and from reflected light on nearby terrain, which can be assumed to be small in the absence of steep topography).

To remove first-order atmospheric effects, a dark shadowed pixel should be chosen in each image to subtract. If this pixel were an ideal shadowed surface with the same albedo, slope, sky exposure, and viewing angle as the sample being corrected, this would nearly cancel out the last two terms in Eq. (1). This is imperfect, because the solid angle of sky seen by a pixel (and therefore the amount of skylight) is different at the edge of shadows compared to deep in the shade. An unshadowed pixel sees even more sky; because martian dust is forward-scattering, much of the scattered atmospheric light comes from the part of the sky close to the Sun, which is cut off in deep shadows. In summary, residual atmospheric contributions to the received radiance are practically unavoidable, and absolute Mars surface albedo measurements are challenging to obtain. We therefore use the following method of relative albedos.

As an approximate dark correction, we use a dark value of 3 DN for every image. This is because HiRISE RDRs are stretched from a DN of 3 to 1021, with the minimum brightness of a 9×9 pixel downsampled image being assigned a value of DN = 3 and the maximum brightness value of the downsampled image assigned to DN = 1021 (Rodney Heyd, personal communication, 12 March 2014). The 9×9 pixel downsampling is performed to identify the true scene minimum, avoiding spurious values due to noise outliers over small pixel areas, such as cosmic ray hits. This is applied to processed image cubes, so all RED CCDs have been normalized to center CCD 5. Thus there should be no differences between measurements taken in different CCDs. This “clipping” means that the lowest DN in any image will always be equal to 3. Therefore instead of finding the darkest shadowed pixel in the scene, we use $DN_{\text{dark}} = 3$ in all cases because by definition the darkest pixel will have a DN value of 3. Unusual circumstances may invalidate this assumption, for example if bit-flip noise creates artificially dark columns in the image. However, we avoided using particularly noisy images, and the worst bit-flipped columns are set to null in the processing. The bit-flip noise in HiRISE images is mainly due to taking images when the Focal Plane Electronics (FPE) are cold, a problem that has increased over the course of the mission (McEwen et al., 2010). The 17% of images in this study with $FPE < 26^\circ\text{C}$ were all taken in the Primary Science Phase, before this problem became more serious over time.

If there are no true shadows in the image, or if the darkest pixel happens to fall on a sloping area and thus is exposed to less sky light, that would also affect the results; this is an additional source of uncertainty in this method.

Using a ratio of two dark-corrected surface samples within a single image nominally eliminates the additional factors in the first term of Eq. (1), assuming the second term has been roughly accounted for. We call this ratio a relative albedo, A_{rel} :

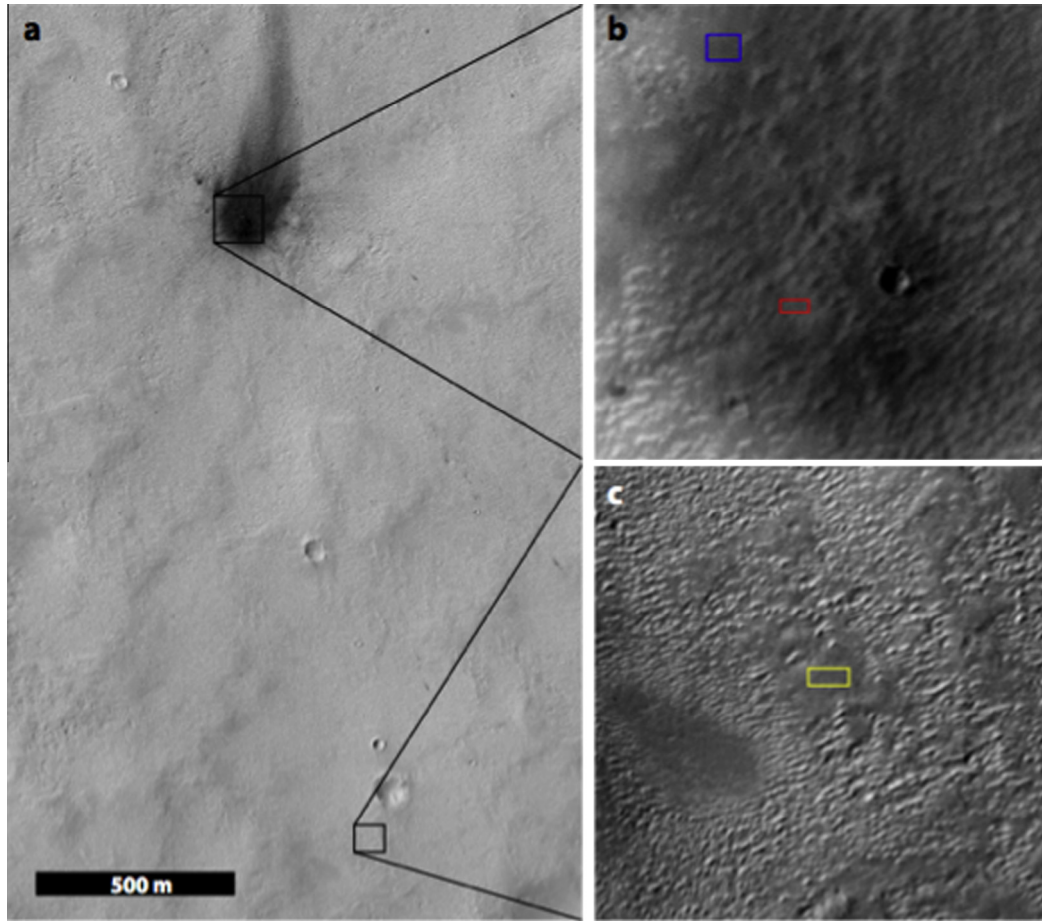


Fig. 7. Example sampling areas used for blast zone relative albedo measurement technique. (a) Context of new impact site. Two regions of interest were selected within the low-albedo blast zone: (b) blue (594 pixels) and red (264 pixels) outlines; and a uniform background sample was chosen far from the impact site: (c) yellow outline (2541 pixels). HiRISE observation ESP_026124_1935 (13.242°N, 15.796°E). (For interpretation of the references to color in this figure legend, the reader is referred to the web version of this article.)

$$A_{\text{rel}} = S_i T_d A_1 T_u / S_i T_d A_2 T_u = A_1 / A_2 \quad (2)$$

where subscripts 1 and 2 indicate the two surface samples in the same image.

To calculate this relative albedo, first the DN values in the HiRISE RDRs must be scaled to a quantitative brightness. HiRISE image DN correspond to a measurement of scene brightness called I/F (Intensity/Flux); this is the ratio of the HiRISE-measured intensity, I_r , to an idealized intensity that would be measured from a perfectly reflecting Lambertian surface illuminated normally at the same distance from the Sun (Eliason et al., 2007). The DN from the RDR products can be converted to I/F according to the values of SCALING_FACTOR and OFFSET stored in the labels:

$$I/F = (\text{DN} \times \text{SCALING_FACTOR}) + \text{OFFSET} \quad (3)$$

(Eliason et al., 2007). Note that this is I/F at the top of the atmosphere.

The dark-pixel values were subtracted from both the BZ and BK values as a first-order atmospheric correction, and the resulting blast zone sample (BZ) values ratioed to the background sample (BK) values:

$$I/F_{\text{rel}} = (I/F_{\text{BZ}} - I/F_{\text{dark}}) / (I/F_{\text{BK}} - I/F_{\text{dark}}) \quad (4)$$

This ratio is equivalent to the ratio of Lambert albedos (A_l) because

$$A_l = I/F_l / \cos(i) \quad (5)$$

and the $\cos(i)$ term can be seen to cancel out in Eqs. (2) and (4), as long as the slope is the same in all areas. Because samples were generally taken on flat surfaces, this is approximately true. The conversion of DN to I/F is linear, so the relative albedo can actually be expressed directly in terms of image DN:

$$A_{\text{rel}} = A_{\text{BZ}} / A_{\text{BK}} = (\text{DN}_{\text{BZ}} - \text{DN}_{\text{dark}}) / (\text{DN}_{\text{BK}} - \text{DN}_{\text{dark}}) \quad (6)$$

Such relative albedos are more accurate than absolute albedos (Delamere et al., 2010) and to first order are independent of lighting conditions. They minimize apparent changes between images due to differing lighting conditions and atmospheric effects. This technique also reduces issues with imperfect absolute radiometric calibration between HiRISE images (Delamere et al., 2010).

The resulting relative albedo was plotted over time (e.g., Fig. 8). Linear fits were made using the LINFIT routine in IDL:

$$A_{\text{rel}} = c_0 + c_1 \Delta d \quad (7)$$

where A_{rel} is the relative albedo as defined above, Δd is the number Earth days elapsed between measurements, and c_0 and c_1 are the coefficients of the best-fit line. That linear trend over time, projected forward to $A_{\text{rel}} = 1$, yields an estimated fading lifetime (L) (from $t = 0$ of the first HiRISE image) for that particular site:

$$L = (1 - c_0) / c_1 \quad (8)$$

The above procedure was performed twice at each site, on the two separate ROIs, and the results were averaged to obtain an estimated lifetime for each site.

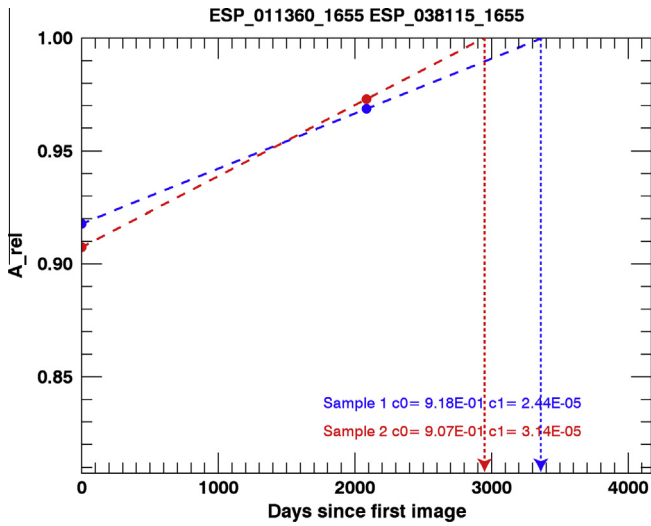


Fig. 8. Example of relative albedo (A_{rel}) plotted over time (Earth days since first image) for the BZ in HiRISE images ESP_011360_1655 and ESP_038115_1655 (-14.41°N , 253.86°E). A linear least-squares fit projected to $A_{rel} = 1$ yields an estimated fading lifetime for each sample at the site, which in this case are 3373 Earth days for sample 1 and 2946 Earth days for sample 2.

Because the original impacts occurred at various times before the first HiRISE image (times that are constrained but not known exactly), these are not absolute lifetimes, but estimates dated from the first HiRISE image. The midpoint of the interval in which the impact could have occurred varies anywhere from a few days to a few years before the initial HiRISE image.

These estimated lifetimes assume fading is linear over time, which may or may not be appropriate. To evaluate that assumption, we examined those sites with more than two observations over multiple Mars years. Least-squares fits were made to a logarithmic function of the form

$$A_{rel} = c_0 \ln(c_1 \Delta d) \quad (9)$$

using the CURVEFIT routine in IDL, and compared to linear fits at the same sites. When this logarithmic fit had a χ^2 value (χ^2 , chi-squared, is a measurement of how well the model fit the

data) less than that for the linear fit, we considered it a better model for that site (Fig. S2), although in some cases neither model fit the data very well. Lifetimes can be calculated using this logarithmic model as well: when A_{rel} is 1, the days elapsed is $\exp[1/c_0]/c_1$. However, these results give unreasonably long lifetimes in many cases (Fig. S2). In reality, this model may apply only to part of the BZs' lifetimes. Fading due to stochastic events like storms will not be fully captured by either model.

4. Results

4.1. Types of changes observed

We observed the following types of changes in BZs, in order of most to least common: (A) Diffuse low-albedo halos fade and approach surrounding albedo (Fig. 9). (B) Extended discrete rays and filamentary features fade, shorten, and disappear (Fig. 10). (C) Dark spots, most commonly smaller outlying ones, disappear completely (Fig. 11). (D) Dust devil tracks and wind streaks appear and disappear (these features are not caused by the impact event, but dust devil tracks are more visible over previously-disturbed areas; Fig. 12). (E) Disappearance of ice and/or blocks near the crater rim. The latter has only been observed at one high-latitude site, which was not included in this study. High-latitude icy crater sites such as that and those discussed previously (Byrne et al., 2009; Dundas and Byrne, 2010) are outside the scope of this study, as the processes involved in their disappearance differ.

4.2. Qualitative intensity of change

Table 1 shows the resulting statistics of qualitative change levels at 106 separate sites. For these statistics, only the first and last images at each site were included, so as not to over-represent sites with more than two repeat images. Almost half (44%) of sites studied for qualitative change showed no change (level 0) or very subtle candidate changes (level 1). Only 19 sites (18% of those studied) showed significant changes such as BZs disappearing completely, despite elapsed times of 1–4 Mars years and indications nearby of other aeolian activity at many of the sites (e.g., dust devil tracks or wind streaks).

We explored correlations between these change rankings and various factors. Correlations are considered to be significant if they

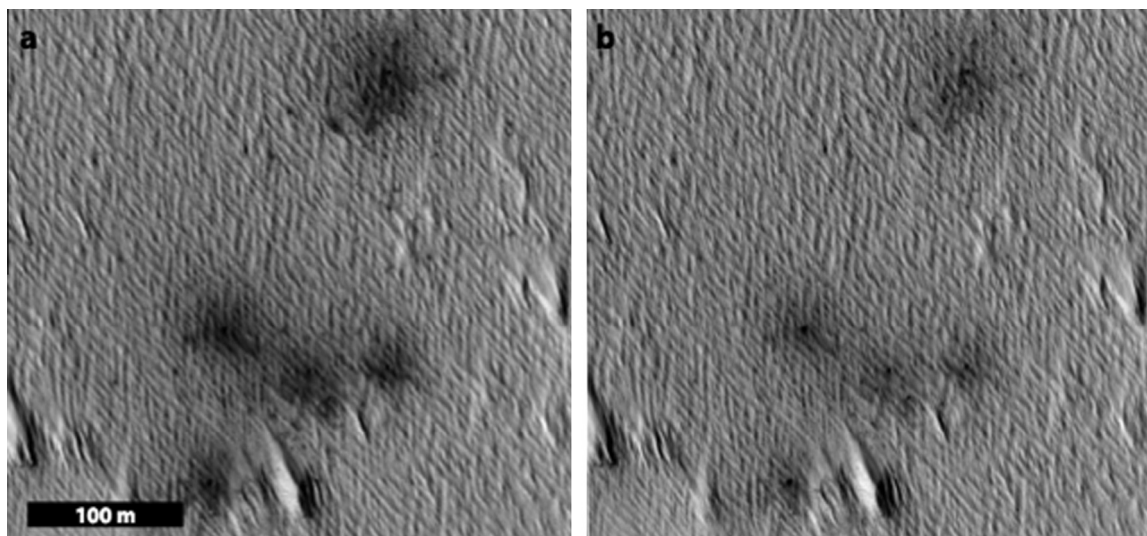


Fig. 9. New dated impact site with low-albedo halos “fading” (increasing in albedo to be closer to albedo of surrounding terrain) over 2 Mars years. Images have been stretched so that color, brightness and contrast of background areas far from impact site match. HiRISE observation IDs (a) PSP_010200_1805 (9/9/2008) and (b) ESP_027685_1805 (6/22/2012) at 0.499°N , 242.327°E .

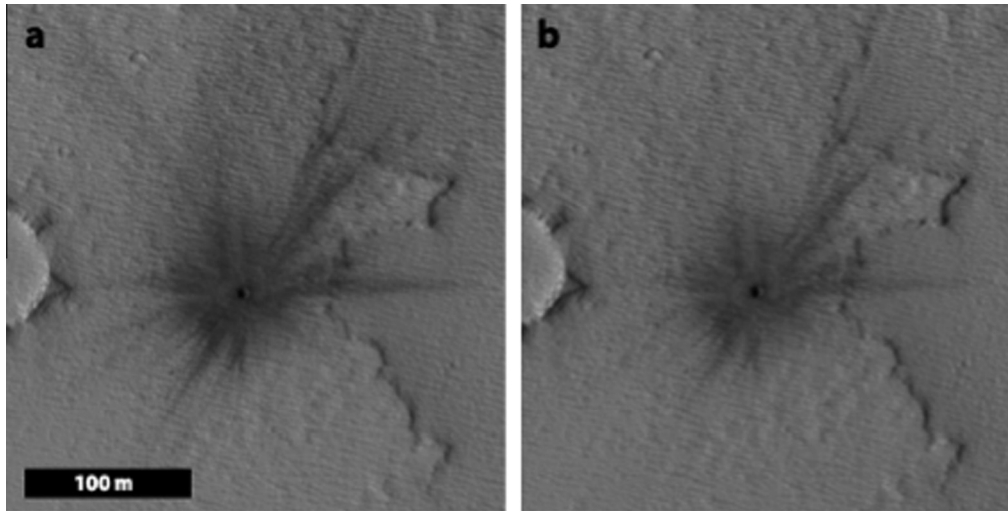


Fig. 10. New dated impact site showing extended low-albedo rays fading and shortening over 2 Mars years. Images have been stretched so that color, brightness and contrast of background areas far from impact site match. HiRISE observation IDs (a) ESP_011584_1785 (1/15/2009) and (b) ESP_029056_1785 (10/7/2012) at -1.568°N , 256.136°E .

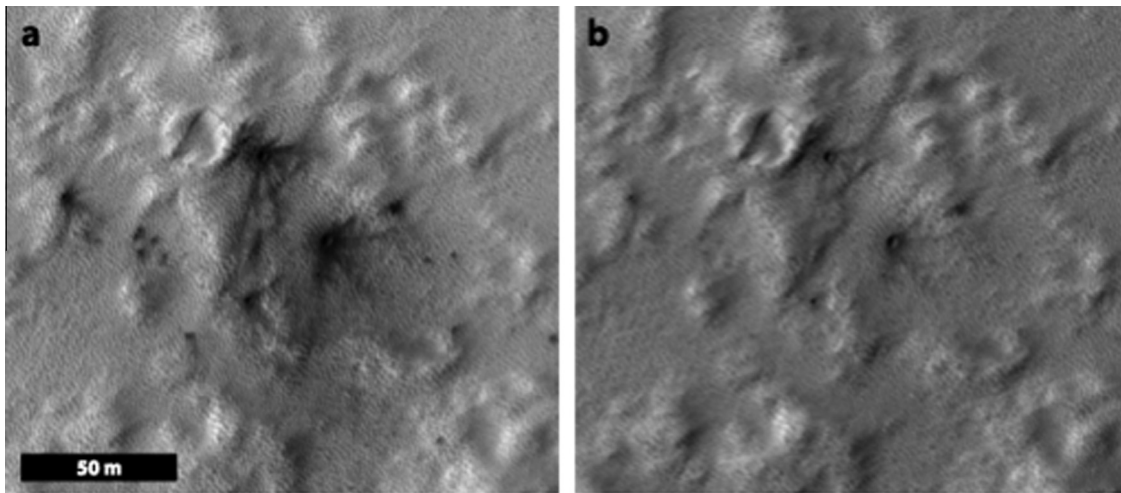


Fig. 11. New dated impact site where low-albedo spots have disappeared over 2 Mars years. HiRISE observation IDs (a) ESP_017637_1875 (5/1/2010) and (b) ESP_035267_1875 (2/3/2014) at 7.295°N , 241.965°E .

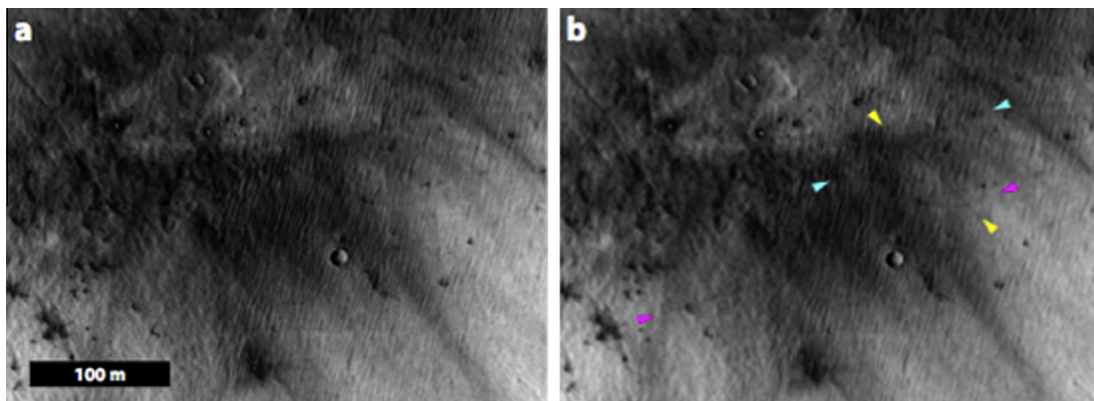


Fig. 12. Dust devil tracks forming at new impact site over 1 martian year. Pairs of arrows in matching colors mark beginnings and ends of several new tracks. The tracks seem to appear over areas already disturbed by the formation of the blast zone, and are not as apparent when they cross higher-albedo areas where dust has not been disturbed. Images have been stretched so that color, brightness and contrast of background areas far from impact site match. HiRISE observation IDs (a) ESP_019926_2070 (10/27/2010) and (b) ESP_028550_2070 (8/29/2012); 26.925°N , 27.3015°E . (For interpretation of the references to color in this figure legend, the reader is referred to the web version of this article.)

Table 1
Results of qualitative change assessment.

Amount of change	# sites	% sites
0 (no change)	11	10
1 (subtle changes)	36	34
2 (definite changes)	40	38
3 (dramatic changes)	19	18

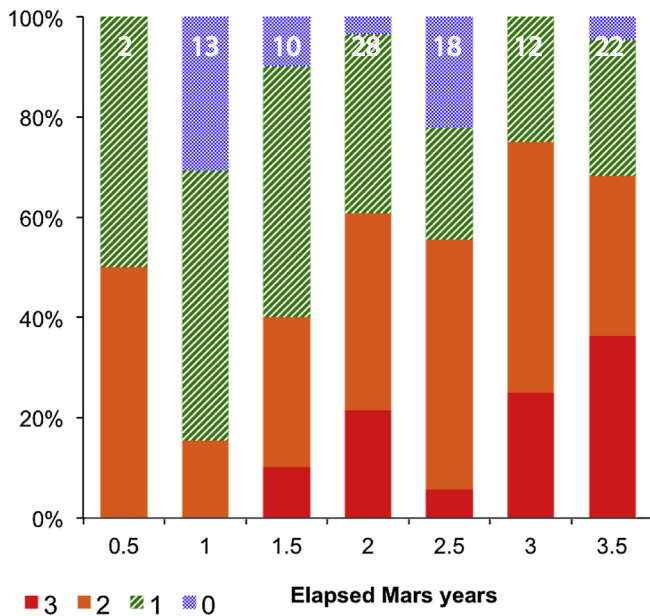


Fig. 13. Stacked histogram of number of sites showing change levels 0 (no changes, blue), 1 (subtle changes, green), 2 (definite changes, orange), and 3 (significant changes, red) at different amounts of elapsed time between images in Mars years. See Section 3.1 for definitions of these change levels. Bins include values less than or equal to their labels; i.e., the right-most bin in this figure includes 3.0–3.5 Mars - years. The total number of sites in each elapsed time bin is shown at the top of each column so that bins with small numbers of sites can be discounted. The data show an increase in the proportion of BZs that have definite and significant changes with increased time. Similarly, the proportion of BZs that show no or subtle changes decreased with increasing time between images. (For interpretation of the references to color in this figure legend, the reader is referred to the web version of this article.)

meet a 95% confidence level. The qualitative change level versus elapsed time (Fig. 13) is correlated, showing more change over longer times, as would be expected. A correlation was found between amount of change and absolute value of latitude, even when the small number of cases at higher latitudes are discounted (Fig. 14). This study excludes very high-latitude sites above 50° absolute latitude where polar processes would be contributing to changes, but we see a correlation with latitude even for sites equatorward of 40°.

Change levels are also correlated with elevation (Fig. 15), with more change seen at lower altitudes. However, if the few sites (5) below -4 km are discounted, the confidence in a correlation with elevation falls to only 86%.

Comparing the amount of change to the Thermal Emission Spectrometer (TES) Dust Cover Index (DCI) (Ruff and Christensen, 2002) (Fig. 16) does not show an overall correlation. Although DCI maps (at 8 pixels per degree) are too coarse to resolve the impact sites described, an elevated level of dust at the surface nearby is not always associated with more changes in BZs. However, for sites that are dusty (DCI < 0.95), there appears to be an increase in the proportion of sites with definite or significant changes with increasing dustiness (decreasing DCI). Interestingly,

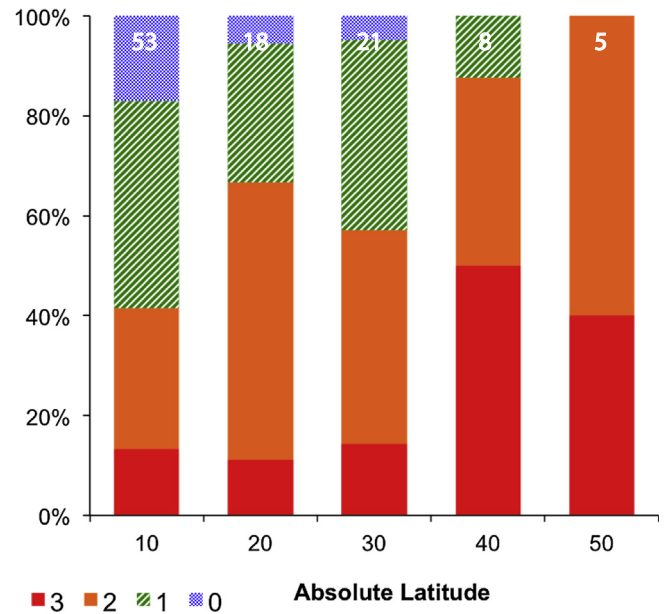


Fig. 14. Stacked histogram of number of sites showing change levels at different absolute values of latitude, plotted as in Fig. 13. More BZs have definite and significant changes at higher latitudes; however, the small sample population of sites at latitudes above 40° makes this uncertain.

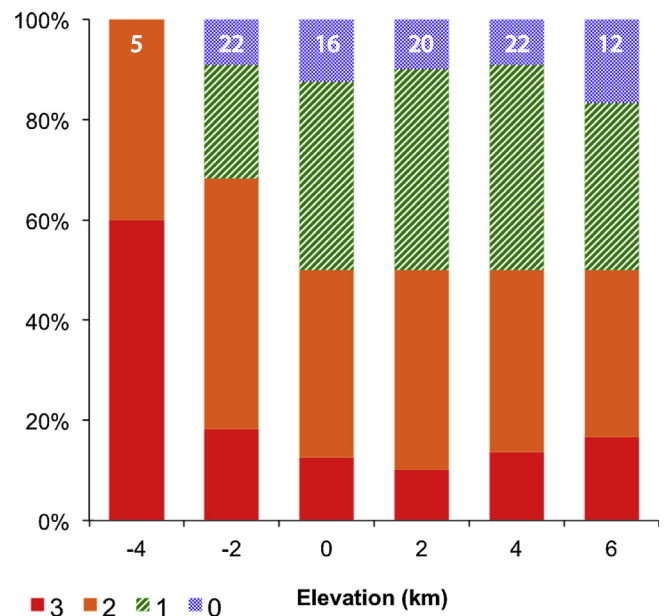


Fig. 15. Stacked histogram of number of sites showing change levels at different elevations, plotted as in Fig. 13. Elevations are from the Mars Orbiter Laser Altimeter (MOLA) 128 ppd global map (Smith et al., 2001). More change is seen at lower elevations: the histogram shows an apparent increase in the proportion of BZs with definite and significant changes with decreasing elevation, but the small sample size at the lowest elevations <-4 km makes this correlation less certain.

for sites that are not dusty (DCI > 0.95), the proportion of sites with definite or significant changes increases with decreasing dustiness, suggesting that the impacts deposited dust at these sites. The small number of less-dusty sites makes this uncertain.

Interestingly, changes seen in BZs show a strong correlation with the effective diameter of the crater at their centers (Fig. 17). Effective diameter refers to the combined diameter for clusters of craters that formed simultaneously, presumably when

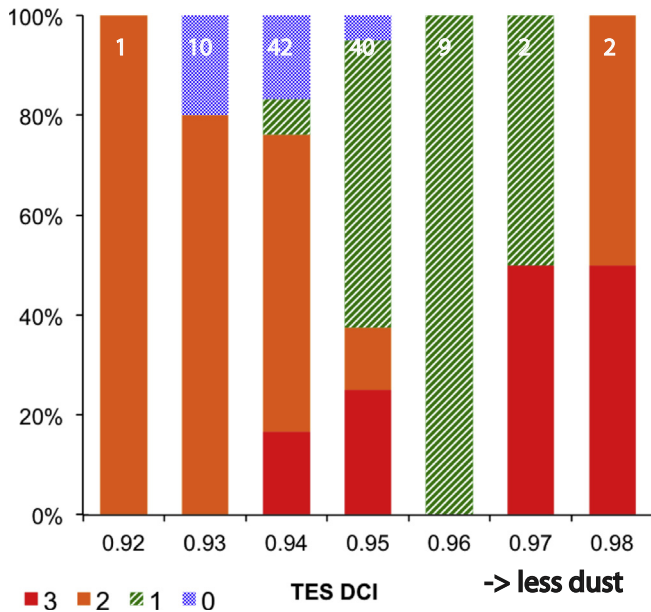


Fig. 16. Stacked histogram of number of sites showing change levels at different values of the TES Dust Cover Index (Ruff and Christensen, 2002), plotted as in Fig. 13. No overall correlation is seen. However, for sites that are dusty (DCI < 0.96), there appears to be an increase in the proportion of sites with definite or significant changes with increasing dustiness (decreasing DCI). Interestingly, for sites that are not dusty (DCI > 0.95), the proportion of sites with definite or significant changes increases with decreasing dustiness, suggesting that the impacts deposited dust at these sites. The small number of less-dusty sites makes this uncertain.

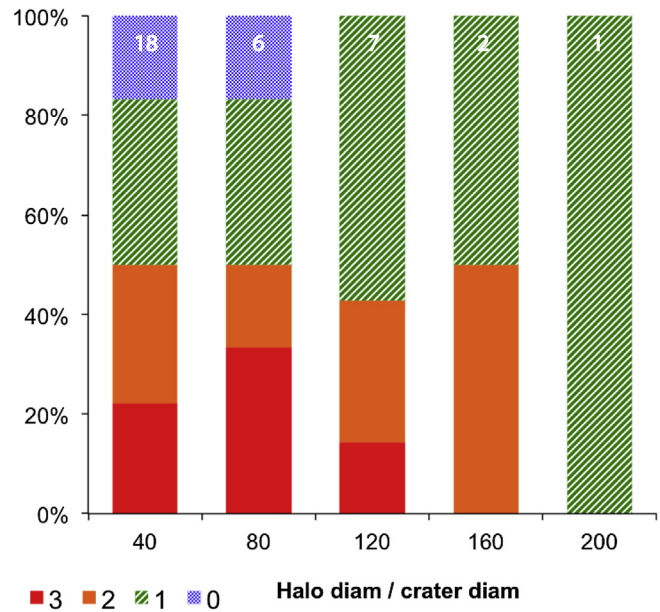


Fig. 18. Stacked histogram of number of sites showing change levels for different values of the ratio between diffuse halo diameter (Bart et al., in preparation) and crater diameter, plotted as in Fig. 13. For clusters, both the crater and halo diameters have been combined to give effective diameters. The amount of change is not correlated to the relative halo size.

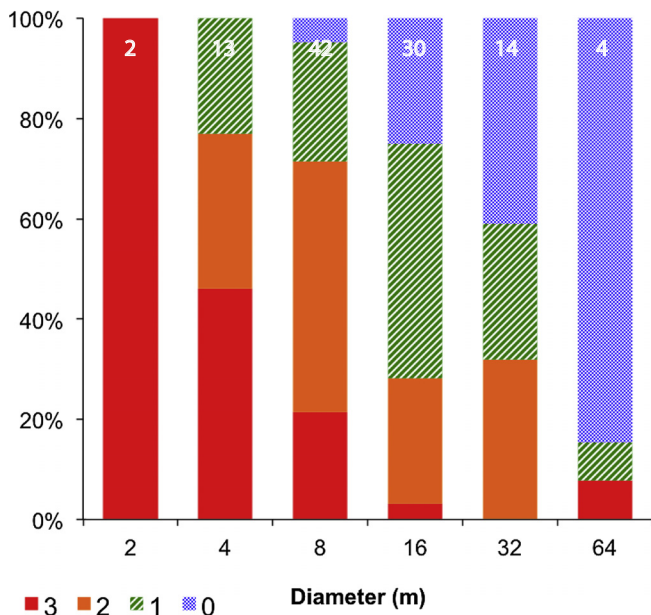


Fig. 17. Stacked histogram of number of sites showing change levels with different diameter craters (effective diameters for clusters), plotted as in Fig. 13. Note that diameter bin sizes are not linear but rather increase by a factor of two for each bin. This histogram shows that the proportion of sites with definite and significant changes increases as crater diameter decreases.

the impactor broke up in the atmosphere, summed as $D_{\text{eff}} = (\sum_i D_i^3)^{1/3}$ (Daubar et al., 2013; Malin et al., 2006). We find that larger impacts show less change over time.

Complementary work (Bart et al., in preparation) examined the sizes of new impact BZs and showed that the diameters of the

diffuse halo portion vary widely with respect to the source crater – from 7 to 220 times the crater size. To measure the halo diameter in that work, a circle was drawn about the entirety of the dark region, leaving no dark area exterior to the circle. The diameter of the circle was taken to be the diameter of the halo. Other features of the BZ such as extended rays are not included in this measurement, which was confined to the smoothly darkened halo region. When comparing halo sizes at the sites where we evaluated changes, no correlation is seen between the relative size of the halo (halo diameter/crater diameter) and the amount of change seen at that site (Fig. 18).

Locations of changes were also compared to historical global albedo changes (Figs. 19 and 20). We compared regional albedo changes in this manner, rather than attempting to compare Global Circulation Models (GCMs), because large-scale models do a poor job of predicting small-scale effects such as locations of current dune activity (Chojnacki et al., 2011) and orientations of dune slip faces (Hayward et al., 2007, 2014).

For this comparison of global albedo changes, we used a time series of global mosaics of Mars (Geissler et al., submitted for publication) produced using data from the MOC wide angle camera (Malin and Edgett, 2001) and Mars Color Imager (MARCI) (Bell et al., 2009). The upper panel of Fig. 19 shows the historical mean red filter radiance at L_s 330°, produced by averaging the mosaics from 2000 to 2009, excluding 2007 when the surface was obscured by a dust storm. The lower panel shows a map of surface changes from 2000 to 2009 produced by summing the absolute values of difference images from 1 Mars year to the next, again at L_s 330° and excluding 2007. In this map, bright areas changed greatly in albedo over this period whereas dark areas changed little. This map is qualitatively similar to, but less pixelated than, a map of the frequency of changes alone, calculated by adding up the number of times the surface brightened or darkened beyond a set threshold. Red symbols in both panels mark dated impact sites in this study that definitely changed (change levels 2 and 3); green symbols mark sites that did not definitively change (change levels 0 and 1). Impact sites that did not change are mostly located in

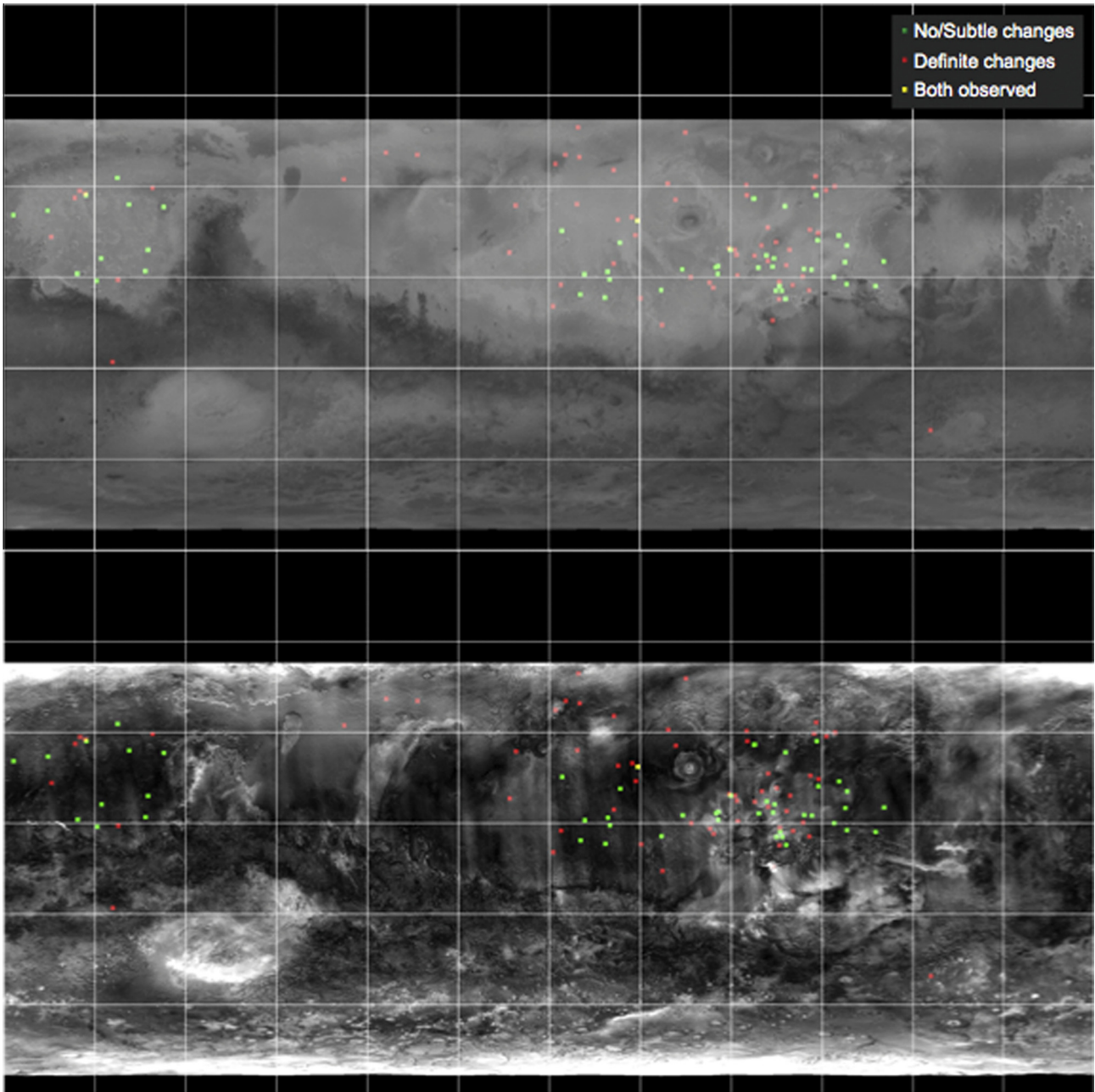


Fig. 19. Locations where qualitative BZ changes were observed (red; levels 2 and 3) compared to historical regional albedo changes. Sites where no or only very subtle changes were observed are marked in green (levels 0 and 1); yellow points mark are where they are co-located. In both panels, the underlying map shows surface albedo changes from 2000 to 2009 derived from MOC wide angle and MARCI data at L_s 330°, excluding 2007 (see text). Upper panel: historical mean red filter radiance produced from averaging the data. Most new impact sites are in areas of high radiance due to the dust cover being required to discover them. Lower panel: surface changes produced by summing the absolute values of difference images from 1 Mars year to the next. Bright areas changed greatly in albedo over this period whereas dark areas changed little. No correlation between BZ changes and historical regional albedo changes is seen. (For interpretation of the references to color in this figure legend, the reader is referred to the web version of this article.)

areas where there were few or minor visible surface albedo changes during 2000–2009. However, the sites that experienced BZ reflectance changes are located in all areas, both in areas with little and areas with pronounced history of regional albedo changes. In addition, sites that changed and sites that did not change are found in close proximity to each other. Finally, no statistical correlation is seen between the historical regional change index and the qualitative amount of change observed (Fig. 20). Therefore we find that the frequency and magnitude of historical regional albedo changes are poor predictors of whether a fresh impact BZ will fade quickly or not.

4.3. Quantitative amount of change

Estimated lower limits on fading lifetimes are shown in Table 2 and Fig. 21. The average minimum predicted lifetime of 116 samples taken at 58 sites is $10,600 \pm 2200$ Earth days, or ~ 15 Mars-years. The average rate of fading is 0.057 ± 0.0045 change in relative albedo per Mars year. There is a wide spread in the lifetimes, and they are skewed toward smaller values (Fig. 21). Demonstrating this, the median lifetime is quite a bit lower than the mean: ~ 5200 Earth days (~ 7.5 Mars years); the mode is 5 Mars years.

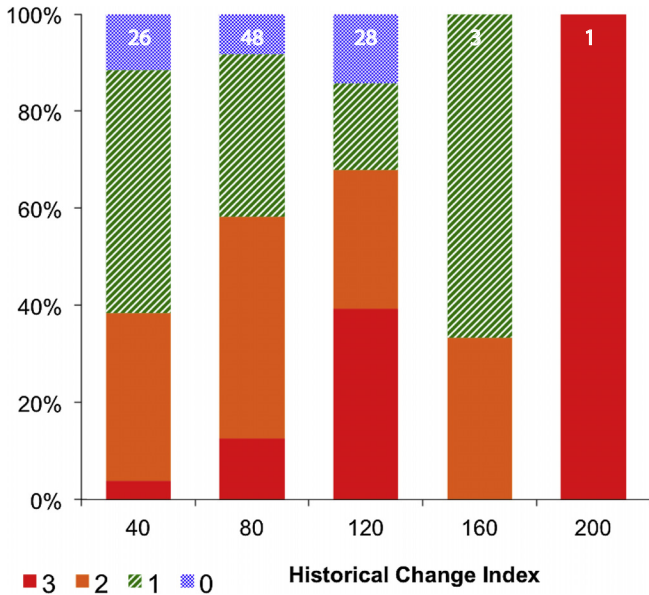


Fig. 20. Stacked histogram of number of sites showing change levels for different values of the historical regional albedo change index shown in Fig. 19, plotted as in Fig. 13. The amount of change is not correlated to the historical regional albedo change.

This analysis does not include those sites whose fading is so slow as to be undetectable. A significant number of new impact sites (12 sites, 17% of all of those quantified) did not have measurable fading timescales (see Fig. 22 for an example). In these cases the linear fits had negative slopes varying from -6×10^{-2} to $-1 \times 10^{-4} A_{rel}/\text{Mars year}$. All of the sites with no measurable fading were in qualitative change categories 0 (no visible changes; 4 sites) or 1 (subtle changes; 8 sites). When including these unchanging sites, the median lifetime increases slightly to ~ 5800 Earth days (~ 8.4 Mars years).

A comparison of the fraction of the fading lifetime elapsed at the time of the image with the qualitative change levels assigned in Section 3.2 show that they are correlated, as would be expected (Fig. 23). Sites with low qualitative change levels (no or only subtle changes) have the lowest values of delta days between images/fading lifetime. This is a measure of the fraction of its lifetime over which it was observed, and so it allows for direct comparison of sites viewed over different timescales (e.g., 1 Mars year vs. three). A site imaged after only 10% of its lifetime had elapsed would be expected to show much less change than a site viewed after 90% of its lifetime. This correlation also serves as a calibration for the qualitative change levels, which could be made at more sites than the quantitative fading measurements.

Nonlinear fits to sites with more than two images (Figs. 24 and S2) show that linear fading is a better model for 44% of the cases (8 out of 18 sites); the remaining sites are fit better by a logarithmic function.

Table 2
Results of quantitative change measurements.

Observation IDs	Sample	Delta days	c_0	c_1	Lifetime (days)	Lifetime (Mars years)	Qual. change category
ESP_026038_2155 ESP_026038_2155	2	701	0.5869	5.02E-04	822	1.20	3
ESP_026038_2155 ESP_026038_2155	1	701	0.6018	3.47E-04	1148	1.67	3
ESP_011428_2200 ESP_011428_2200	2	1373	0.7539	1.76E-04	1400	2.04	3
ESP_013707_1915 ESP_013707_1915	1	1351	0.7544	1.55E-04	1588	2.31	3
ESP_017637_1875 ESP_017637_1875	2	1374	0.6471	1.85E-04	1907	2.78	3
ESP_011698_1810 ESP_011698_1810	1	1356	0.7272	1.43E-04	1910	2.78	0
ESP_013707_1915 ESP_013707_1915	2	1351	0.7532	1.18E-04	2088	3.04	3
ESP_017637_1875 ESP_017637_1875	1	1374	0.5482	1.71E-04	2646	3.85	3
ESP_018707_2205 ESP_018707_2205	1	1357	0.3641	2.25E-04	2827	4.12	3
PSP_004175_2060 PSP_004175_2060	2	1454	0.5771	1.49E-04	2837	4.13	2
ESP_011360_1655 ESP_011360_1655	2	2085	0.9074	3.14E-05	2946	4.29	3
PSP_004123_1915 PSP_004123_1915	2	1366	0.5491	1.46E-04	3086	4.49	1
PSP_010319_1780 PSP_010319_1780	1	2063	0.6303	1.19E-04	3102	4.52	3
ESP_011428_2200 ESP_011428_2200	1	1373	0.6266	1.18E-04	3158	4.60	3
ESP_017803_2080 ESP_017803_2080	2	1357	0.5643	1.31E-04	3332	4.85	2
ESP_011360_1655 ESP_011360_1655	1	2085	0.9178	2.44E-05	3373	4.91	3
ESP_011584_1785 ESP_011584_1785	1	1361	0.6199	1.11E-04	3432	5.00	2
ESP_026124_1935 ESP_026124_1935	2	717	0.5381	1.32E-04	3500	5.09	2
ESP_017492_1890 ESP_017492_1890	1	1369	0.5020	1.40E-04	3548	5.16	2
ESP_016239_2060 ESP_016239_2060	1	1374	0.7691	6.45E-05	3578	5.21	1
PSP_010740_1840 PSP_010740_1840	2	2063	0.4702	1.47E-04	3607	5.25	3
PSP_010740_1840 PSP_010740_1840	1	2063	0.4876	1.40E-04	3663	5.33	3
ESP_017492_1890 ESP_017492_1890	2	1369	0.4705	1.42E-04	3720	5.41	2
ESP_016239_2060 ESP_016239_2060	2	1374	0.7697	6.13E-05	3758	5.47	1
PSP_004175_2060 PSP_004175_2060	1	1454	0.3973	1.59E-04	3784	5.51	2
PSP_003780_2000 PSP_003780_2000	2	1393	0.5979	1.06E-04	3784	5.51	2
ESP_011584_1785 ESP_011584_1785	2	1361	0.5765	1.12E-04	3796	5.53	2
ESP_017038_1790 ESP_017038_1790	1	1385	0.3207	1.78E-04	3818	5.56	2
PSP_004123_1915 PSP_004123_1915	1	1366	0.4987	1.31E-04	3830	5.58	1
ESP_026124_1935 ESP_026124_1935	1	717	0.5466	1.16E-04	3914	5.70	2
ESP_018707_2205 ESP_018707_2205	2	1357	0.3767	1.50E-04	4148	6.04	3
ESP_026248_2280 ESP_026248_2280	2	657	0.6527	8.30E-05	4185	6.09	2
ESP_013287_1845 ESP_013287_1845	1	1384	0.6853	7.51E-05	4189	6.10	2
PSP_008015_2205 PSP_008015_2205	2	2087	0.6571	8.09E-05	4240	6.17	2
ESP_013287_1845 ESP_013287_1845	2	1384	0.6314	8.18E-05	4506	6.56	2
PSP_008015_2205 PSP_008015_2205	1	2087	0.6332	7.96E-05	4606	6.70	2
PSP_006787_2045 PSP_006787_2045	2	2088	0.7718	4.87E-05	4689	6.83	3
ESP_017038_1790 ESP_017038_1790	2	1385	0.4471	1.18E-04	4700	6.84	2

Table 2 (continued)

Observation IDs	Sample	Delta days	c_0	c_1	Lifetime (days)	Lifetime (Mars years)	Qual. change category
ESP_026248_2280 ESP_026248_2280	1	657	0.5872	8.58E-05	4808	7.00	2
PSP_006787_2045 PSP_006787_2045	1	2088	0.7665	4.56E-05	5122	7.46	3
PSP_003925_1940 PSP_003925_1940	1	2077	0.5299	9.10E-05	5164	7.52	2
ESP_011623_2100 ESP_011623_2100	2	2073	0.6788	6.20E-05	5183	7.54	3
ESP_017803_2080 ESP_017803_2080	1	1357	0.4481	1.03E-04	5371	7.82	2
ESP_014010_1800 ESP_014010_1800	1	1395	0.5232	8.25E-05	5779	8.41	2
ESP_012441_1775 ESP_012441_1775	1	1356	0.6042	6.80E-05	5824	8.48	2
ESP_011623_2100 ESP_011623_2100	1	2073	0.5938	6.93E-05	5859	8.53	3
PSP_003527_1940 PSP_003527_1940	1	2077	0.6303	6.12E-05	6044	8.80	1
PSP_003780_2000 PSP_003780_2000	1	1393	0.5458	7.41E-05	6128	8.92	2
PSP_007499_1810 PSP_007499_1810	1	680	0.8761	1.98E-05	6270	9.13	0
ESP_014010_1800 ESP_014010_1800	2	1395	0.4980	7.78E-05	6455	9.40	2
PSP_003925_1940 PSP_003925_1940	2	2077	0.5102	7.51E-05	6522	9.49	2
ESP_012441_1775 ESP_012441_1775	2	1356	0.6218	5.72E-05	6615	9.63	2
PSP_010319_1780 PSP_010319_1780	2	2063	0.4119	8.58E-05	6851	9.97	3
PSP_005942_1825 PSP_005942_1825	2	2044	0.7804	2.97E-05	7395	10.76	1
PSP_005942_1825 PSP_005942_1825	1	2044	0.7488	2.98E-05	8417	12.25	1
ESP_016238_1850 ESP_016238_1850	2	1374	0.6995	3.47E-05	8666	12.61	1
PSP_002736_2075 PSP_002736_2075	2	2049	0.7412	2.95E-05	8768	12.76	1
PSP_010621_1960 PSP_010621_1960	2	1368	0.5561	4.89E-05	9073	13.21	2
PSP_006629_1955 PSP_006629_1955	2	2032	0.8258	1.80E-05	9694	14.11	1
PSP_010621_1960 PSP_010621_1960	1	1368	0.5491	4.35E-05	10,367	15.09	2
PSP_003527_1940 PSP_003527_1940	2	2077	0.6329	3.38E-05	10,856	15.80	1
ESP_016238_1850 ESP_016238_1850	1	1374	0.6941	2.80E-05	10,907	15.88	1
PSP_002736_2075 PSP_002736_2075	1	2049	0.7163	2.59E-05	10,952	15.94	1
PSP_003101_2065 PSP_003101_2065	1	2049	0.4923	4.46E-05	11,392	16.58	2
PSP_003101_2065 PSP_003101_2065	2	2049	0.6016	3.18E-05	12,549	18.27	2
PSP_007036_1765 PSP_007036_1765	1	2093	0.6980	2.32E-05	13,037	18.98	2
PSP_008300_1905 PSP_008300_1905	1	2076	0.7283	1.95E-05	13,931	20.28	1
PSP_007009_1905 PSP_007009_1905	1	2060	0.6392	2.50E-05	14,403	20.97	2
ESP_011698_1810 ESP_011698_1810	2	1356	0.7410	1.72E-05	15,067	21.93	0
PSP_007036_1765 PSP_007036_1765	2	2093	0.7792	1.43E-05	15,468	22.52	2
PSP_007009_1905 PSP_007009_1905	2	2060	0.7505	1.57E-05	15,876	23.11	2
ESP_014150_2130 ESP_014150_2130	2	1395	0.6385	2.03E-05	17,821	25.94	1
PSP_010147_1830 PSP_010147_1830	1	684	0.6950	1.46E-05	20,865	30.37	1
PSP_008300_1905 PSP_008300_1905	2	2076	0.7002	1.44E-05	20,887	30.40	1
PSP_007378_1860 PSP_007378_1860	1	2082	0.7550	1.11E-05	22,129	32.21	0
PSP_007246_1890 PSP_007246_1890	2	675	0.6276	1.32E-05	28,255	41.13	2
PSP_006629_1955 PSP_006629_1955	1	2032	0.8304	5.96E-06	28,451	41.42	1
PSP_007499_1810 PSP_007499_1810	2	680	0.8656	4.42E-06	30,379	44.22	0
ESP_014150_2130 ESP_014150_2130	1	1395	0.6418	1.18E-05	30,459	44.34	1
PSP_007246_1890 PSP_007246_1890	1	675	0.5818	1.19E-05	35,082	51.07	2
PSP_007378_1860 PSP_007378_1860	2	2082	0.6664	1.85E-06	180,091	262.15	0
PSP_010147_1830 PSP_010147_1830	2	684	0.7034	1.57E-06	188,520	274.42	1
PSP_007879_1725 PSP_007879_1725 ESP_016674_1725	1	2059	0.6486	9.34E-05	3762	5.48	3
PSP_007879_1725 PSP_007879_1725 ESP_016674_1725	2	2059	0.6576	7.67E-05	4467	6.50	3
PSP_009265_1730 PSP_009265_1730 ESP_017480_1730	1	2075	0.6507	1.07E-04	3251	4.73	3
PSP_009265_1730 PSP_009265_1730 ESP_017480_1730	2	2075	0.7547	1.03E-04	2379	3.46	3
PSP_002764_1800 PSP_002764_1800 ESP_019154_1800	1	2727	0.7497	3.83E-05	6543	9.52	2
PSP_002764_1800 PSP_002764_1800 ESP_019154_1800	2	2727	0.7512	3.62E-05	6875	10.01	2
PSP_007272_1945 PSP_007272_1945 ESP_016291_1945	1	1382	0.7336	2.95E-05	9030	13.15	2
PSP_007272_1945 PSP_007272_1945 ESP_016291_1945	2	1382	0.7759	3.90E-05	5743	8.36	2
PSP_003602_2085 PSP_003602_2085 ESP_013267_2085	1	2049	0.5674	4.69E-05	9219	13.42	2
PSP_003602_2085 PSP_003602_2085 ESP_013267_2085	2	2049	0.5143	3.41E-05	14,254	20.75	2
ESP_011368_1860 ESP_011368_1860 ESP_028840_1860	1	2090	0.5760	2.91E-05	14,594	21.24	1
ESP_011368_1860 ESP_011368_1860 ESP_028840_1860	2	2090	0.6149	4.98E-05	7733	11.26	1
PSP_010331_1755 PSP_010331_1755 ESP_019113_1755	1	2063	0.7327	2.62E-05	10,215	14.87	2
ESP_019113_1755							
PSP_010331_1755 PSP_010331_1755 ESP_019113_1755	2	2063	0.7268	2.15E-05	12,711	18.50	2
ESP_019113_1755							
PSP_010528_1770 PSP_010528_1770 ESP_028290_1770	1	2096	0.7982	3.38E-05	5973	8.69	1
PSP_010528_1770 PSP_010528_1770 ESP_028290_1770	2	2096	0.7756	3.90E-05	5749	8.37	1
PSP_010200_1805 PSP_010200_1805 ESP_027685_1805	1	2075	0.6220	1.09E-04	3481	5.07	3
PSP_010200_1805 PSP_010200_1805 ESP_027685_1805	2	2075	0.5680	9.05E-05	4771	6.95	3
PSP_010862_1880 PSP_010862_1880 ESP_029046_1880	1	2080	0.4612	1.07E-04	5055	7.36	2
PSP_010862_1880 PSP_010862_1880 ESP_029046_1880	2	2080	0.4840	1.01E-04	5124	7.46	2
PSP_010634_2135 PSP_010634_2135 ESP_019482_2135	1	2047	0.6306	8.45E-05	4373	6.37	2
ESP_019482_2135							
PSP_010634_2135 PSP_010634_2135 ESP_019482_2135	2	2047	0.7409	6.21E-05	4171	6.07	2
ESP_019482_2135							
PSP_010255_1700 PSP_010255_1700 ESP_027806_1700	1	2091	0.5724	7.62E-05	5610	8.17	2
PSP_010255_1700 PSP_010255_1700 ESP_027806_1700	2	2091	0.9102	5.89E-05	1524	2.22	2
ESP_011491_2090 ESP_011491_2090 ESP_028963_2090	1	2068	0.5350	3.68E-05	12,649	18.41	2
ESP_011491_2090 ESP_011491_2090 ESP_028963_2090	2	2068	0.5657	4.41E-05	9860	14.35	2

(continued on next page)

Table 2 (continued)

Observation IDs	Sample	Delta days	c_0	c_1	Lifetime (days)	Lifetime (Mars years)	Qual. change category
ESP_019195_2175 ESP_019195_2175 ESP_027964_2175	1	1362	0.6169	2.15E-04	1786	2.60	3
ESP_019195_2175 ESP_019195_2175 ESP_027964_2175	2	1362	0.6248	2.12E-04	1772	2.58	3
ESP_019287_2295 ESP_019287_2295 ESP_028201_2295	1	1401	0.6501	1.98E-04	1767	2.57	3
ESP_019287_2295 ESP_019287_2295 ESP_028201_2295	2	1401	0.6407	1.58E-04	2274	3.31	3
ESP_019926_2070 ESP_019926_2070 ESP_028550_2070	1	1407	0.6160	5.92E-05	6483	9.44	1
ESP_019926_2070 ESP_019926_2070 ESP_028550_2070	2	1407	0.6307	5.71E-05	6472	9.42	1
ESP_020854_1965 ESP_020854_1965 ESP_029834_1965	1	1356	0.7055	1.06E-04	2769	4.03	2
ESP_020854_1965 ESP_020854_1965 ESP_029834_1965	2	1356	0.7573	1.11E-04	2190	3.19	2

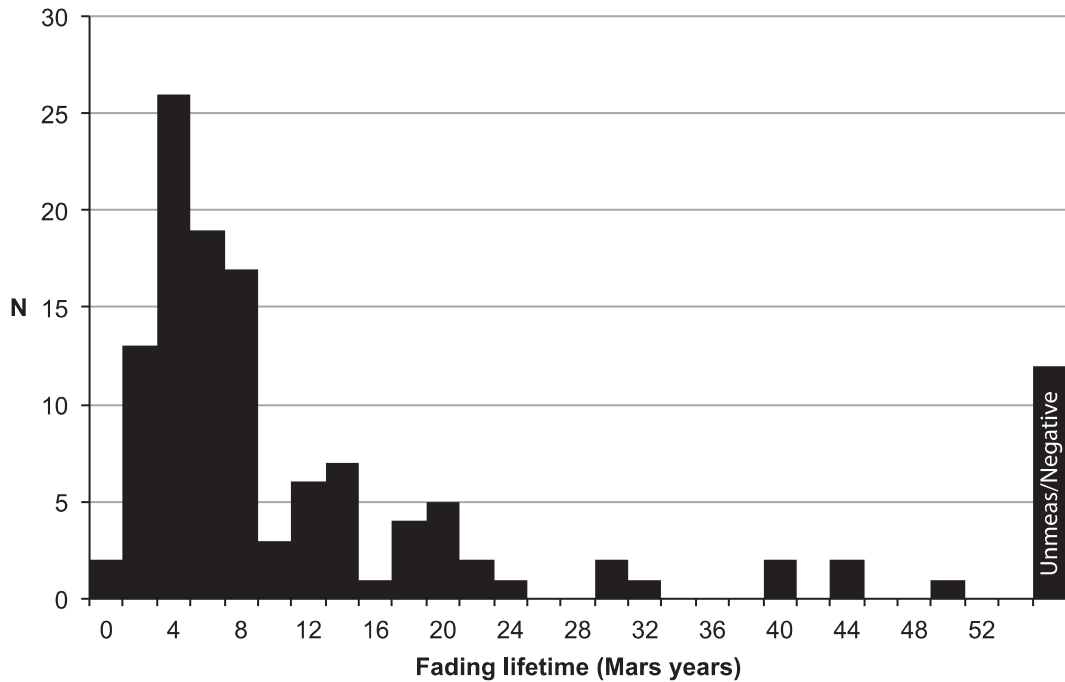


Fig. 21. Histogram of minimum estimated lifetimes (in Mars years) of new impact blast zones, assuming linear fading over time. Sites with lifetimes that cannot be constrained (negative relative albedo slopes over time) are grouped at the right of the histogram. The average lifetime of 58 measurable sites is 15 Mars years, the mode is 5 Mars years, and the median lifetime of all 70 sites including those with unmeasurable fading is 8 Mars years.

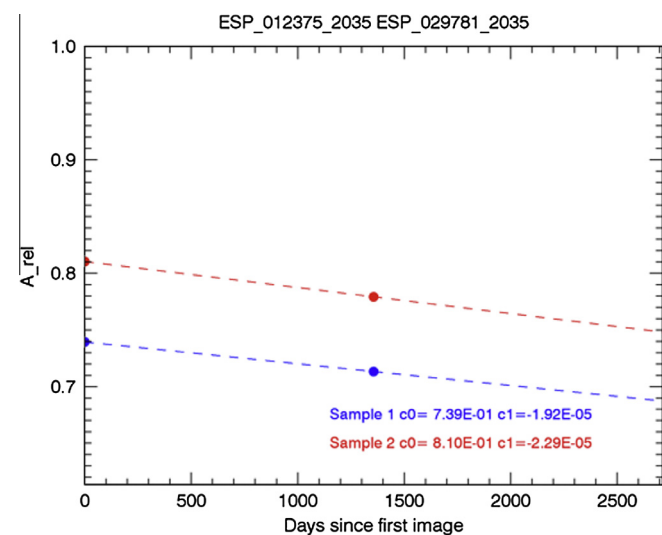


Fig. 22. Example of site where fading lifetime could not be determined: a linear fit to the relative albedo (A_{rel}) over time has a negative slope (c_1). This could be the result of unreliable albedo measurements, changes that are smaller than the errors in our method, or a true decrease in albedo at this site.

5. Discussion

5.1. Sites with undetectable change and possible darkening

Sites where the fading rate could not be measured (e.g., Fig. 22) could be cases where the albedo measurements are not reliable, or they could be the result of very subtle, extremely slow fading, such that the change in A_{rel} is within the errors inherent in our method. We have observed examples of much older impacts, unconstrained with ‘before’ images, where the BZ has appeared to persist since Viking Orbiter images from the late 1970s (e.g., HiRISE observation ID PSP_002183_1970 at 17.03°N, 246.40°E; this is also a much larger crater than any of those studied here).

It is also possible that some process is actually darkening the BZs at these sites. This is seen directly in some areas of extreme cases, such as the eastern portion of the impact site shown in Fig. 5. Perhaps the impact disturbs some sand-sized particles as well as dust, which saltate over time and further erode the high-albedo dust, or the disturbed area is prone to having what dust remains after impact later lifted away by e.g., dust devils. Updrafts could be more common over darkened areas that are consequently warmer. This would be consistent with the more distinct dust devil tracks within the BZ in Fig. 12. Although we did avoid obvious dust

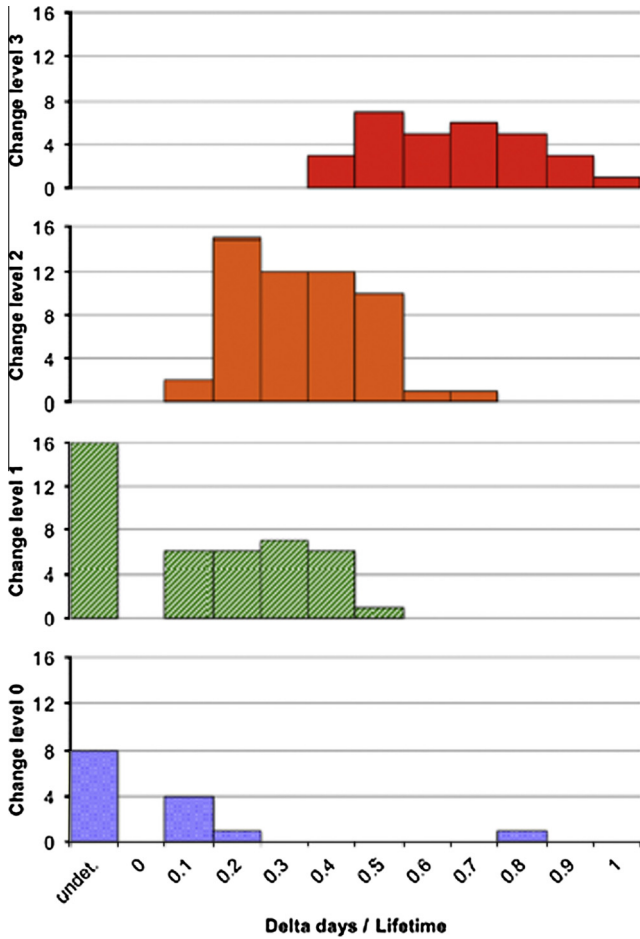


Fig. 23. Histograms of number of samples (two per site) observed at a given fraction of their estimated fading lifetimes (delta days between images/lifetime in days), for each qualitative change level. This is a measure of the fraction of its lifetime over which it was observed, and so it allows for direct comparison of sites viewed over different timescales. Sites with undetectable fading, and thus lifetimes that cannot be estimated, are shown at left of histograms.

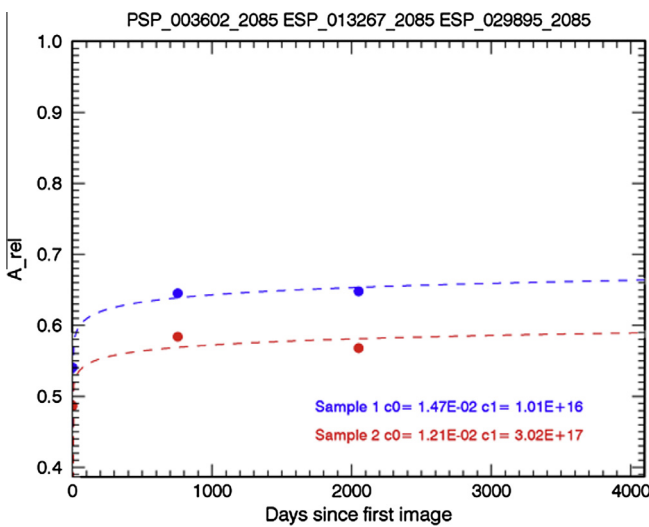


Fig. 24. Example of non-linear fits to fading behavior of a site with three images. Relative albedo (A_{rel}) is plotted against time (days since the first image). Logarithmic functions of the form $A_{rel} = c_0 \ln(c_1 t)$ were used. The model fit shows a rapid initial fading, followed by slow fading over longer timescales. Similar plots for all sites are in supplemental material (Fig. S2).

devil tracks, very subtle ones could have been unknowingly included in the albedo measurements.

The prevalence of non-linear fading as a better fit to the data might be related to these apparently slowly-fading sites. The non-linear model is physically reasonable, given that albedo obscuration by dust accumulation should resemble optical depth in the atmosphere, which behaves exponentially (the Beer–Lambert Law). (Surface roughness effects may produce different behavior.) This logarithmic fading may apply only to a portion of the BZ lifespan; more extended observations will clarify that behavior. Sampling a BZ during the very slowly-changing latter portion of its lifespan may give results such as these. Alternatively, perhaps the background albedo consists of many such areas that are nearly, but not quite completely, faded, such that no absolute background albedo exists. To some extent the behavior may be stochastic or seasonal, reflecting the effects of dust storms and other major weather events like seasonally high winds.

5.2. Factors determining rates of change

Qualitative changes in BZs correlate with several factors: more change is seen (1) over longer periods of time, (2) at higher latitudes, (3) lower elevations, and where (4) craters are smaller.

Greater amounts of change over time (factor 1) is unsurprising; the longer the time that has elapsed since the impact, the more time processes have had to act on the impacted surfaces. The correlation with latitude (factor 2) could be the result of enhanced seasonal processes at high latitudes; although we excluded sites above 50° absolute latitude, that is not an absolute cutoff for seasonal processes. Thus the highest latitude bins in Fig. 14 may be affected by such processes, although the correlation persists even below 40° latitude. This may be a result of interconnected factors, such as the generally lower elevations at high northern latitudes.

The correlation we see with elevation (factor 3) is not surprising because atmospheric pressure varies by a factor of 9.2 over the 24 km range in elevation our sites span, using a scale height of 10.8 km; (Zurek, 1992). A denser atmosphere might be expected to more efficiently redistribute surface dust and increase saltation of surrounding sand. Thus this correlation can be explained if the thicker atmosphere at lower elevations causes BZs to equilibrate with their surroundings more rapidly.

Finally, the correlation with crater size (factor 4) implies that larger impacts create albedo patterns that change more slowly and last longer.

5.3. Implications for processes forming and erasing BZs

Surprisingly, many of the new impact BZs show no detectable qualitative changes or measurable fading after up to 4 martian years – even over intervals including the 2007 global dust storm in some cases, various regional and local dust-raising events in others, and areas with large regional historical albedo changes. Although no new bedform formation or movement (e.g., ripple migration) has been detected near these sites, as has been found in other areas of Mars (Bridges et al., 2012, 2013; Chojnacki et al., 2014), dust devil tracks, wind streaks, and features resembling spire streaks (Toyota et al., 2011) are observed to form and disappear between repeat images. This raises the question of what structure the albedo features could have that has no resolvable topographic expression, yet persists despite nearby aeolian activity and presumably ongoing dust deposition. It is not known, for instance, whether the dark tone of BZs is due to exposure or deposition of dark material with a composition or grain size different from the surrounding surface, versus unresolved shadows, surface roughness differences, or other textural effects. We therefore compare formation and erasure processes with those of other

low-albedo features that fade over time: slope streaks, dust devil tracks, and rover tracks.

The high energy of a hypervelocity impact might be expected to cause more permanent or deeper modification than the force that darkens the surface associated with rover wheels or dust avalanches, although the thin atmosphere may not exert much force depending on the details of the airblast. This hypothesis is supported by the correlation we find between size of craters (*i.e.*, energy of impact) and the qualitative lifetimes of the corresponding BZs: larger craters show less change. Thus those sites with the most energetic formation processes are the longest-lived. However, the formation mechanism for BZs must not involve appreciable erosion or deposition. The BZs do not appear to have any relief higher than a few centimeters that HiRISE is able to detect, and other than a few isolated examples of ejecta blocks near the rim, there is no evidence in HiRISE images for deep scouring, thick deposition, or other topographic disturbance of the surface at 1-m and larger scales. In comparison, rover wheel tracks vary in depth from zero to ~ 1 cm (Geissler et al., 2010), which might be a similar range of depth given that any topographic expression within the BZs is lower than HiRISE's ability to detect it. Slope streaks, which were initially thought to be mere albedo markings, were found with HiRISE images to have detectable depths ≤ 1 m (Chuang et al., 2007). However, the favored model for slope streak formation, gravity-driven avalanching of dust (Baratoux et al., 2006; Sullivan et al., 2001), is not likely to have an analogy at most impact sites except in the special cases where the BZ is largely composed of slope streaks. Dust devils exhibit tangential wind speeds of 20–30 m/s (Choi and Dundas, 2011), enough to lift ~ 2 μm of dust (Greeley et al., 2003), but do not leave any topographic signatures; these may be analogous to processes in impact blasts, but are likely to have much lower energy.

The processes of erasure might also differ between new impact BZs and these other features. The average quantitative lifetime of BZs is comparable to that of slope streaks, which fade gradually over ~ 20 Mars years (Bergonio et al., 2013; Schorghofer et al., 2007). In comparison, dust devil (Balme et al., 2003; Verba et al., 2010) and rover tracks (Geissler et al., 2010) fade much more quickly, on timescales of a few months to 1 Mars year. Of these albedo phenomena, slope streaks have the most similar lifetimes, but they are probably not a good analogy for the impact BZs because they have different appearances (*e.g.*, slope streaks have sharp edges while BZs are diffuse) and formation mechanisms. Slope streaks have been reported to have albedo contrasts with their surroundings of only up to 10% (Sullivan et al., 2001) or in another single example, 25% (Mushkin et al., 2010). However, those results neglected to make atmospheric corrections. Corrected albedo measurements using HiRISE images show slope streaks to have albedo contrasts (darkening) up to $\sim 50\%$ of their surroundings in one example image (McEwen et al., 2014, Supplementary material). The new impact BZs seem to have similar contrast: they are 40–90% of the albedo of the unmodified surroundings when initially imaged, the majority being 60–80% (Fig. 25). This suggests similar amounts of dust removal by impacts and slope streaks.

The differences in quantitative lifetimes imply that either the processes erasing BZs around new impacts are different from those acting on dust devil or rover tracks, or the magnitude of the effect differs. Gradual cover from airfall dust is thought to be the mechanism of fading for dust devil tracks (Greeley et al., 2003, 2005) as well as slope streaks (Chuang et al., 2010; Sullivan et al., 2001). A dust coating tens to a few hundred microns thick would be enough to cover a surface with an optically thick layer, depending on wavelength and grain size (Dundas and Byrne, 2010; Fischer and Pieters, 1993; Morris et al., 2001; Wells et al., 1984). Dust deposition from atmospheric fallout has been estimated to occur at rates ranging from 0 to 250 $\mu\text{m}/\text{Earth year}$ (Aharonson, 2003;

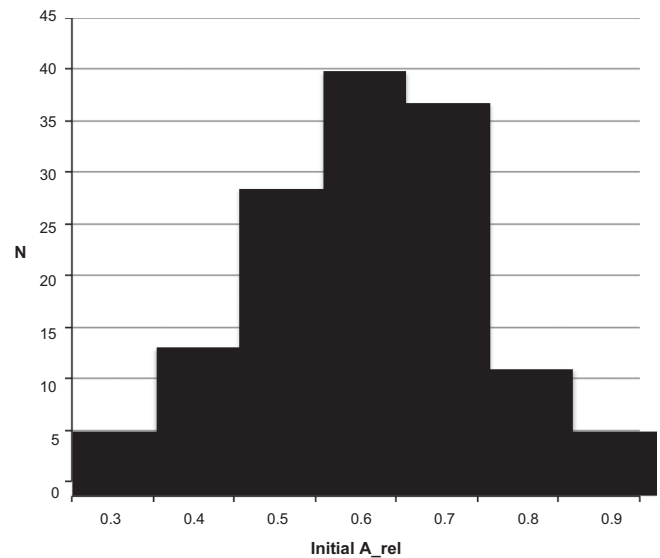


Fig. 25. Initial relative albedos of blast zones: Number of blast zone samples (two per impact site) with a given albedo relative to the background surroundings, A_{rel} , at the time of the initial HiRISE image at the site. Histogram shows that initial albedo of BZs averages 65% that of the surroundings; the median is 64%, and the mode is 60%.

Christensen, 1986; Golombek et al., 2006; Kinch et al., 2007; Pollack et al., 1979). These estimates vary by more than three orders of magnitude, and include zero, so they do not constrain BZ erasure rates well. There are also surely spatial and temporal variations present in the deposition rate, as seen with MER (Kinch et al., 2007), and as suggested to explain variable fading rates of slope streaks (Aharonson, 2003). Using a moderate airfall rate of 6.7 $\mu\text{m}/\text{Earth year}$ (Pollack et al., 1979), it would take ~ 6 Earth years to accumulate a 40 μm thick layer, enough to be optically opaque at the wavelengths of the HiRISE red filter (Dundas and Byrne, 2010). It would take ~ 60 Earth years if a 400 μm thick layer were required to shield the dark substrate (Morris et al., 2001). On the other end of the spectrum, using the early mission measurements of airfall dust deposited on the calibration targets of the MER rovers before any dust-clearing events occurred (Kinch et al., 2007), an optical depth of one would be deposited in only 1 Earth year. These timescales vary widely, but are roughly comparable to the lifetimes we estimate from BZ fading rates, so gradual airfall of dust is a possible fading mechanism. However, that cannot be the sole explanation for the qualitative changes that are seen. The situation is not as simple as depositing an opaque layer of bright dust everywhere, because that would effectively mask both the core and fringes of dark spots, when we observe them shrinking but not disappearing completely. So other processes must be occurring as well. For example, perhaps the darkening is due to surface roughness effects with amplitudes that vary across the diameter of the BZ. (This may also be favored by the longer lifetimes of BZs around larger impacts, if more energetic impacts create rougher surfaces.) If this were the case, a small amount of deposition could smooth, and thus brighten, the outer part of the BZ first, where the vertical roughness is smallest. A mix of erosion and deposition is also possible, for example if wind eroded high-standing topography and deposition of dust filled in low-standing areas, together these could act to reset the surface.

We also consider the possibility that fading is being caused by some mechanism other than dust airfall. In the case of rover tracks, erasure was found in some cases to be caused by deposition of and erosion by near-surface aeolian transport (Geissler et al., 2010); dust storms and dust devil passages also contributed to Spirit's

tracks fading in some areas (Geissler et al., 2010). Aeolian sediment transport has been found to be effective on minimum length scales of hundreds of meters (Geissler et al., 2010), the same size scale of many of the BZs. These transport processes seem to work more rapidly on rover tracks, which disappear in ~ 1 Mars year, or more quickly if associated with an event such as a dust storm or dust devil passage (Geissler et al., 2010). Why do these processes not erase BZs on similarly short timescales? Perhaps at impact sites the loose sediments that would otherwise be transported to cover the BZs over short ranges have already been removed by the impact blast itself to farther distances, thus preventing the erasure that would otherwise occur from its redistribution. Alternatively, meteorological conditions at the sites of the rover tracks may have been more favorable to those transportation processes than is generally true over the rest of Mars. Another possibility is that material of an appropriate size for saltation is rare in the dust-covered areas where new impacts are most commonly detected.

Future work could investigate changing roughness and its effect on reflectance at these sites. The BZs at lunar spacecraft landing sites have been studied in this manner, ratioing images taken at different phase angles to calculate surface roughness (Clegg et al., 2014; Kaydash et al., 2011; Kaydash and Shkuratov, 2012, 2014; Shkuratov et al., 2013). However, this type of analysis requires images taken at varying phase angles, which are not available for the majority of the new impact sites.

5.4. Implications for measurements of modern cratering rate

One question we aimed to address with this study was whether the current impact rate measurement using BZs (Daubar et al., 2013) suffers from under-sampling due to missing sites that faded before they could be imaged by CTX. The high fraction (44%) of sites showing no or only minor qualitative changes (level 0 or 1) and the long average quantitative fading lifetime implies that fading of BZs does not lead to an overall low measured impact rate. We can quantify this by comparing the median fading lifetime (8.4 Mars years) to the average time between all overlapping before-and-after CTX images used in the Daubar et al. (2013) study, which is 0.7 Mars years. Not one of the sites in this study had a fading lifetime less than this average CTX repeat time—the fastest-fading site had an estimated lifetime of 1.2 Mars years, almost twice as long. Of course, if any sites do fade extremely quickly, before CTX can provide initial post-image coverage, then they would not be discovered and cannot be included in this analysis.

One caveat is that (especially with nonlinear fading), it is not necessary to reach 100% of the fading lifetime before a blast zone becomes visually indistinct to CTX. This is especially true if the BZ shrinks over time as fainter outer areas fade first. However, the median lifetime is more than a factor of ten larger than the average CTX overlap time, so this does not fundamentally change our conclusion that in general, the fading appears to be much slower than the typical repeat time of CTX images, indicating CTX is most likely not missing many new impacts in the dusty areas of Mars. The Daubar et al. (2013) method of calculating the current impact rate uses only CTX–CTX-constrained impacts; this avoids fading issues that could be present if longer-spaced repeat imaging were considered as well, for example MOC–CTX or Viking–CTX detections.

A second caveat is that if there are sites that systematically fade quickly, for example in matters of days, they are unlikely to be included in the data set studied here. Our quantitative fading rate measurements are only made at sites that were discovered, *i.e.*, relatively slowly fading sites by definition. However, given the number of sites and time period included, it seems likely that some examples of this type of behavior should have been observed, where the site was imaged just before it rapidly faded and disappeared.

There is at least one example of extremely rapid change: the BZ in ESP_039861_1225 (-57.343°N , 125.169°E) faded completely by the time of ESP_040784_1225 (72 days later). Although this is at a higher latitude than any of our study sites, the images were both in summer ($L_s = 280^{\circ}$ and 323° , respectively), so this disappearance could not be due to winter seasonal processes, and the crater probably post-dated the seasonal cap from the previous spring. This year (Mars year 32, July 2013–June 2015; Piqueux et al., 2015) was also an unusually active one for south polar dust storms, so this may be a rare case. However, it is at least possible that there are some quickly-fading BZs at low latitudes that experience modification processes in common with this site.

Of particular interest is any process preventing recognition of smaller impacts, which may explain the shallowness of the measured size frequency distribution (SFD) compared to that predicted by popular production functions (Daubar et al., 2013). This is in fact indicated by the prevalence of changes seen around smaller craters (Fig. 17). The shallower SFD may be partly explained by faster fading of BZs for small impacts, causing more small impacts to not be discovered in the first place. This may not explain the entire difference in slope between the measured SFD and model predictions if atmospheric effects are contributing to loss of small craters.

6. Conclusions

Many new martian impact blast zones have changed drastically over relatively short timescales. Surprisingly, however, approximately half of the new impact sites show little to no change, despite being freshly disturbed surfaces in areas with evidence of recent aeolian activity and other albedo changes. The qualitative amount of change observed is correlated with the amount of time elapsed, latitude, elevation, and effective crater diameter. From this we infer that processes responsible for BZ fading and eventual disappearance seem to be dependent on atmospheric pressure (sites with higher pressure fade faster) and the energy of the impact that formed the BZ (sites with larger central craters fade more slowly). No correlation is found between the amount of change and dust cover or size of the diffuse halo relative to the crater. The historical frequency of regional albedo changes as seen in MOC and MARCI data also cannot be used to predict whether a BZ will fade quickly. Changes may be due to the stochastic occurrence of local dust storms.

Quantitative changes in albedo yield estimated lifetimes of BZs. In about half of the cases with three or more repeat images, nonlinear fading is a better model. In such cases linear fits to the data yield minimum estimated lifetimes. These minimum lifetimes vary widely, but average 15 Mars years and have a median of 8 Mars years. Therefore similar “dark-spot” impacts lacking age constraints from prior imaging are likely to be on the order of decades old or younger. The average lifetime of BZs is comparable to that of slope streaks, but significantly longer than dust devil or rover tracks. Thus fading of BZs is more representative of global atmospheric dust deposition, rather than the more quickly-acting aeolian processes that erase other albedo features on recently-disturbed dusty surfaces. While airflow of high-albedo dust is the most likely mechanism for erasure of BZs, other processes are also involved; in particular processes of deposition and erosion may be working in combination to erase these features.

These lifetimes indicate the measurement of the current impact rate based on BZ detections (Daubar et al., 2013) is accurate, as that method utilized only sites with CTX data for both before and after images; *i.e.*, that production function has not vastly under-sampled new impacts due to fading prior to detection. However, the prevalence of changes seen around smaller craters may explain in part the shallower slope of that size frequency distribution compared to model predictions.

Acknowledgments

We are grateful for the HiRISE operations staff for acquiring and processing the excellent data used in this study, and the CTX operations team for discovering candidate new impact sites. Our thanks go to Rod Heyd for answering questions about the detailed processing of HiRISE RDRs and Guy McArthur for help with the HiView software. Patricio Becerra also provided useful discussion. We appreciate the helpful comments from Moses Milazzo and two anonymous reviewers, especially one reviewer whose thoughtful and detailed comments greatly improved this work. This work was partially supported by an appointment to the NASA Postdoctoral Program at the Jet Propulsion Laboratory, California Institute of Technology, administered by Oak Ridge Associated Universities through a contract with the National Aeronautics and Space Administration.

Appendix A. Supplementary material

Supplementary data associated with this article can be found, in the online version, at <http://dx.doi.org/10.1016/j.icarus.2015.11.032>.

References

- Aharonson, O., 2003. Slope streak formation and dust deposition rates on Mars. *J. Geophys. Res.* 108, 5138. <http://dx.doi.org/10.1029/2003JE002123>.
- Balme, M.R., Whelley, P.L., Greeley, R., 2003. Mars: Dust devil track survey in Argyre Planitia and Hellas Basin. *J. Geophys. Res.* 108, 5086. <http://dx.doi.org/10.1029/2003JE002096>.
- Baratoux, D. et al., 2006. The role of the wind-transported dust in slope streaks activity: Evidence from the HRSC data. *Icarus* 183, 30–45. <http://dx.doi.org/10.1016/j.icarus.2006.01.023>.
- Bell, J.F. et al., 2009. Mars Reconnaissance Orbiter Mars Color Imager (MARCI): Instrument description, calibration, and performance. *J. Geophys. Res.* 114, E08S92. <http://dx.doi.org/10.1029/2008JE003315>.
- Bergoniu, J.R., Rottas, K.M., Schorghofer, N., 2013. Properties of martian slope streak populations. *Icarus* 225, 194–199. <http://dx.doi.org/10.1016/j.icarus.2013.03.023>.
- Bridges, N.T. et al., 2012. Planet-wide sand motion on Mars. *Geology* 40, 31–34. <http://dx.doi.org/10.1130/G32373.1>.
- Bridges, N. et al., 2013. Bedform migration on Mars: Current results and future plans. *Aeolian Res.* <http://dx.doi.org/10.1016/j.aeolia.2013.02.004>.
- Burleigh, K.J. et al., 2012. Impact airblast triggers dust avalanches on Mars. *Icarus* 217, 194–201. <http://dx.doi.org/10.1016/j.icarus.2011.10.026>.
- Byrne, S. et al., 2009. Distribution of mid-latitude ground ice on Mars from new impact craters. *Science* (80-) 325, 1674–1676. <http://dx.doi.org/10.1126/science.1175307>.
- Calef, F.J., Herrick, R.R., Sharp, V.L., 2009. Geomorphic analysis of small rayed craters on Mars: Examining primary versus secondary impacts. *J. Geophys. Res.* 114, E10007. <http://dx.doi.org/10.1029/2008JE003283>.
- Cantor, B.A., 2007. MOC observations of the 2001 Mars planet-encircling dust storm. *Icarus* 186, 60–96. <http://dx.doi.org/10.1016/j.icarus.2006.08.019>.
- Choi, D.S., Dundas, C.M., 2011. Measurements of martian dust devil winds with HiRISE. *Geophys. Res. Lett.* 38. <http://dx.doi.org/10.1029/2011GL049806>.
- Chojnacki, M. et al., 2011. Orbital observations of contemporary dune activity in Endeavour crater, Meridiani Planum, Mars. *J. Geophys. Res.* 116, E00F19. <http://dx.doi.org/10.1029/2010JE003675>.
- Chojnacki, M., Johnson, J., Michaels, T., 2014. Persistent aeolian activity at Endeavour Crater, Meridiani Planum. *Lunar Planet. Sci.* 45, Abstract 2775.
- Christensen, P.R., 1986. Regional dust deposits on Mars: Physical properties, age, and history. *J. Geophys. Res.* 91, 3533–3545. <http://dx.doi.org/10.1029/JB091iB03p03533>.
- Chuang, F.C. et al., 2007. HiRISE observations of slope streaks on Mars. *Geophys. Res. Lett.* 34, L20204. <http://dx.doi.org/10.1029/2007GL031111>.
- Chuang, F.C., Beyer, R.A., Bridges, N.T., 2010. Modification of martian slope streaks by aeolian processes. *Icarus* 205, 154–164. <http://dx.doi.org/10.1016/j.icarus.2009.07.035>.
- Clegg, R.N. et al., 2014. Effects of rocket exhaust on lunar soil reflectance properties. *Icarus* 227, 176–194. <http://dx.doi.org/10.1016/j.icarus.2013.09.013>.
- Daubar, I.J. et al., 2013. The current martian cratering rate. *Icarus* 225, 506–516. <http://dx.doi.org/10.1016/j.icarus.2013.04.009>.
- Daubar, I., McEwen, A.S., Golombek, M.P., 2015. Albedo changes at martian landing sites. *Lunar Planet. Sci.* 46, Abstract 2225.
- Delamere, W.A. et al., 2010. Color imaging of Mars by the High Resolution Imaging Science Experiment (HiRISE). *Icarus* 205, 38–52. <http://dx.doi.org/10.1016/j.icarus.2009.03.012>.
- Dundas, C.M., Byrne, S., 2010. Modeling sublimation of ice exposed by new impacts in the martian mid-latitudes. *Icarus* 206, 716–728. <http://dx.doi.org/10.1016/j.icarus.2009.09.007>.
- Dundas, C. et al., 2014. HiRISE observations of new impact craters exposing martian ground ice. *J. Geophys. Res.: Planets*, 109–127. <http://dx.doi.org/10.1002/2013JE004482>. Received.
- Eliason, E. et al., 2007. Software Interface Specification for HiRISE Reduced Data Record Products. JPL Document D-32006. <http://hirise.lpl.arizona.edu/pdf/HiRISE_RDR_SIS.pdf>.
- Fischer, E., Pieters, C., 1993. The continuum slope of Mars: Bidirectional reflectance investigations and applications to Olympus Mons. *Icarus* 102, 185–202.
- Geissler, P., Daubar, I., 2010. Eolian degradation of young martian craters. *Lunar Planet. Sci. Abstract* 2009–2010.
- Geissler, P.E., Enga, M.T., Mukherjee, P., submitted for publication. Orbital monitoring of martian surface changes. *Icarus*.
- Geissler, P.E. et al., 2010. Gone with the wind: Eolian erasure of the Mars Rover tracks. *J. Geophys. Res.* 115, E00F11. <http://dx.doi.org/10.1029/2010JE003674>.
- Geissler, P.E. et al., 2013. Shifting sands on Mars: Insights from tropical intra-crater dunes. *Earth Surf. Process. Landforms* 38, 407–412. <http://dx.doi.org/10.1002/esp.3331>.
- Golombek, M.P. et al., 2006. Erosion rates at the Mars Exploration Rover landing sites and long-term climate change on Mars. *J. Geophys. Res.* 111, E12S10. <http://dx.doi.org/10.1029/2006JE002754>.
- Greeley, R. et al., 2003. Martian dust devils: Laboratory simulations of particle threshold. *J. Geophys. Res.* 108, 5041. <http://dx.doi.org/10.1029/2002JE001987>.
- Greeley, R. et al., 2005. Martian variable features: New insight from the Mars Express Orbiter and the Mars Exploration Rover Spirit. *J. Geophys. Res.* 110, E06002. <http://dx.doi.org/10.1029/2005JE002403>.
- Hayward, R.K. et al., 2007. Mars Global Digital Dune Database and initial science results. *J. Geophys. Res.: Planets* 112, 1–17. <http://dx.doi.org/10.1029/2007JE002943>.
- Hayward, R.K., Fenton, L.K., Titus, T.N., 2014. Mars Global Digital Dune Database (MGD3): Global dune distribution and wind pattern observations. *Icarus* 230, 38–46. <http://dx.doi.org/10.1016/j.icarus.2013.04.011>.
- Ivanov, B., Melosh, H., Mcewen, A.S., 2010. New small impact craters in high resolution HiRISE images – III. Lunar Planet. Sci. Abstract 2020.
- Johnson, J.R. et al., 2012. Surface changes observed at Greeley Haven during Opportunity's fifth martian winter. *American Geophysical Union* (Fall), Abstract 2–3.
- Johnson, J.R. et al., 2015. ChemCam passive reflectance spectroscopy of surface materials at the Curiosity landing site, Mars. *Icarus* 249, 74–92. <http://dx.doi.org/10.1016/j.icarus.2014.02.028>.
- Kaydash, V.G., Shkuratov, Y.G., 2012. Structural disturbances of the lunar surface caused by spacecraft. *Solar Syst. Res.* 46, 108–118. <http://dx.doi.org/10.1134/S0038094612020050>.
- Kaydash, V.G., Shkuratov, Y.G., 2014. Structural disturbances of the lunar surface near the Lunokhod-1 spacecraft landing site. *Solar Syst. Res.* 48, 167–175. <http://dx.doi.org/10.1134/S0038094614030034>.
- Kaydash, V. et al., 2011. Photometric anomalies in the Apollo landing sites as seen from the Lunar Reconnaissance Orbiter. *Icarus* 211, 89–96. <http://dx.doi.org/10.1016/j.icarus.2010.08.024>.
- Kinch, K.M. et al., 2007. Dust deposition on the Mars Exploration Rover Panoramic Camera (Pancam) calibration targets. *J. Geophys. Res.* 112, E06S03. <http://dx.doi.org/10.1029/2006JE002807>.
- Malin, M.C., Edgett, K.S., 2001. Mars Global Surveyor Mars Orbiter Camera: Interplanetary cruise through primary mission. *J. Geophys. Res.* 106, 23429. <http://dx.doi.org/10.1029/2000JE001455>.
- Malin, M.C. et al., 2006. Present-day impact cratering rate and contemporary gully activity on Mars. *Science* (80-) 314, 1573–1577. <http://dx.doi.org/10.1126/science.1135156>.
- Malin, M.C. et al., 2007. Context Camera Investigation on board the Mars Reconnaissance Orbiter. *J. Geophys. Res.* 112, E05S04. <http://dx.doi.org/10.1029/2006JE002808>.
- McEwen, A.S. et al., 2007. Mars Reconnaissance Orbiter's High Resolution Imaging Science Experiment (HiRISE). *J. Geophys. Res.: Planets* 112, 1–40. <http://dx.doi.org/10.1029/2005JE002605>.
- McEwen, A.S. et al., 2010. The High Resolution Imaging Science Experiment (HiRISE) during MRO's Primary Science Phase (PSP). *Icarus* 205, 2–37. <http://dx.doi.org/10.1016/j.icarus.2009.04.023>.
- McEwen, A.S. et al., 2014. Recurring slope lineae in equatorial regions of Mars. *Nat. Geosci.* 7, 53–58. <http://dx.doi.org/10.1038/ngeo2014>.
- Mehta, M. et al., 2011. Explosive erosion during the Phoenix landing exposes subsurface water on Mars. *Icarus* 211, 172–194. <http://dx.doi.org/10.1016/j.icarus.2010.10.003>.
- Mellon, M.T. et al., 2009. The periglacial landscape at the Phoenix landing site. *J. Geophys. Res.* 114, E00E06. <http://dx.doi.org/10.1029/2009JE003418>.
- Morris, R.V. et al., 2001. Effects of palagonitic dust coatings on visible, near-IR, and Mössbauer spectra of rocks and minerals: Implications for mineralogical remote sensing of Mars. *Lunar Planet. Sci.* 32, Abstract 1912.
- Mushkin, A., Gillespie, A.R., Montgomery, D.R., Schreiber, B.C., Arvidson, R.E., 2010. Spectral constraints on the composition of low-albedo slope streaks in the Olympus Mons Aureole. *Geophys. Res. Lett.* 37, L22201.
- Piqueux, S. et al., 2015. Enumeration of Mars years and seasons since the beginning of telescopic exploration. *Icarus* 251, 332–338. <http://dx.doi.org/10.1016/j.icarus.2014.12.014>.

- Pollack, J.B. et al., 1979. Properties and effects of dust particles suspended in the martian atmosphere. *J. Geophys. Res.* 84, 2929. <http://dx.doi.org/10.1029/JB084iB06p02929>.
- Ruff, S.W., Christensen, P.R., 2002. Bright and dark regions on Mars: Particle size and mineralogical characteristics based on Thermal Emission Spectrometer data. *J. Geophys. Res.* 107, 5127. <http://dx.doi.org/10.1029/2001JE001580>.
- Schorghofer, N. et al., 2007. Three decades of slope streak activity on Mars. *Icarus* 191, 132–140. <http://dx.doi.org/10.1016/j.icarus.2007.04.026>.
- Shkuratov, Y. et al., 2013. Lunar surface traces of engine jets of Soviet sample return probes: The enigma of the Luna-23 and Luna-24 landing sites. *Planet. Space Sci.* 75, 28–36. <http://dx.doi.org/10.1016/j.pss.2012.10.016>.
- Silvestro, S. et al., 2010. Ripple migration and dune activity on Mars: Evidence for dynamic wind processes. *Geophys. Res. Lett.* 37, L20203. <http://dx.doi.org/10.1029/2010GL044743>.
- Smith, E. et al., 2001. Mars Orbiter Laser Altimeter: Experiment summary after the first year of global mapping of Mars. *J. Geophys. Res.: Planets* 106, 689–722.
- Sullivan, R. et al., 2001. Mass movement slope streaks imaged by the Mars Orbiter Camera. *J. Geophys. Res.* 106, 23607. <http://dx.doi.org/10.1029/2000JE001296>.
- Toyota, T., Kurita, K., Spiga, a., 2011. Distribution and time-variation of spire streaks at Pavonis Mons on Mars. *Planet. Space Sci.* 59, 672–682. <http://dx.doi.org/10.1016/j.pss.2011.01.015>.
- Verba, C. et al., 2010. Observations from the High Resolution Imaging Science Experiment (HiRISE): Martian dust devils in Gusev and Russell craters. *J. Geophys. Res.* 115, E09002. <http://dx.doi.org/10.1029/2009JE003498>.
- Wells, E.N., Veverka, J., Thomas, P., 1984. Mars – Experimental study of albedo changes caused by dust fallout. *Icarus* 58, 331–338. [http://dx.doi.org/10.1016/0019-1035\(84\)90079-4](http://dx.doi.org/10.1016/0019-1035(84)90079-4).
- Zurek, R., 1992. Comparative aspects of the climate of Mars: An introduction to the current atmosphere. In: Kieffer, H. et al. (Eds.), *Mars*. University of Arizona Press, Tucson, AZ, pp. 799–817.
- Zurek, R.W., Smrekar, S.E., 2007. An overview of the Mars Reconnaissance Orbiter (MRO) science mission. *J. Geophys. Res.: Planets* 112, 1–22. <http://dx.doi.org/10.1029/2006JE002701>.